ISSN 2096-7071 (Print)
ISSN 2097-3101 (Online)
CN 10-1629/R1

CHINA CDC WEEKLY

Vol. 8 No. 9 Feb. 27, 2026

中国疾病预防控制中心周报(英文)

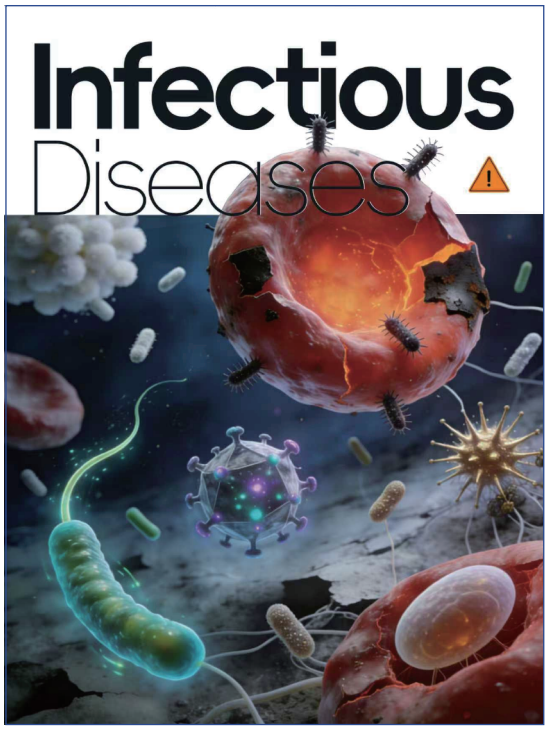

ISSN 2096-7071
9 772096 707262 09>

China CDC Weekly

Editorial Board

Editorial Office

Cover Image: credited from Beijing Shengyue Yongdong Education Technology Co., Ltd.

Vital Surveillances

Genomic Epidemiology of *Salmonella enterica* Serovar Give Reveals Clonal Expansion and Increasing Prevalence of *qnrB19* — China, 2017–2024

Bowei Sun[1]; Fenxia Fan[1]; Zhigang Cui[1]; Xiaoli Du[1]; Jieren Wang[1]; Haijian Zhou[1]; Biao Kan[1]; Meiying Yan[1,#]

ABSTRACT

Introduction: Most current research on *Salmonella* has targeted prevalent serotypes, such as *S.* Typhimurium and *S.* Enteritidis, but the epidemiology and molecular characteristics of less prevalent serotypes remain insufficiently characterized. This study focused on *S.* Give, a less common serotype, to elucidate its genomic characteristics and antimicrobial resistance gene (ARG) profiles in China.

Methods: The whole-genome sequences of 185 isolates of *S.* Give were extracted from the Chinese Pathogen Identification Network database from 2017 to 2024 and subjected to ARG detection and phylogenetic analysis.

Results: Two major sequence types (STs) were identified among the *S.* Give isolates, with ST516 being the predominant ST (92.43%) in China — consistent with the global ST distribution, except in the U.S., where ST654 prevailed (82.70%). The multidrug resistance (concurrent carriage of ≥3 ARGs) rate was 3.51%. All 185 isolates harbored the T57S point mutation in the *parC* gene on the chromosome, and an increasing trend was observed in the quinolone resistance gene *qnrB19* prevalence in China from 2020 to 2024. In the major sublineage, 80% of the isolates contained the *qnrB19* gene, and 86.41% of the isolates carried the small mobilizable plasmid Col (pHAD28) harboring the *qnrB19* gene. Six clusters were detected, indicating several potential outbreaks within China. Moreover a close phylogenetic relationship with European strains was exhibited.

Conclusion: This study shows that *S.* Give predominates in China and is characterized by clonal expansion and the widespread presence of *qnrB19*-harboring plasmids. *S.* Give's sporadic outbreaks and multidrug resistance represent emerging public health threats. Moreover, the ongoing genomic surveillance of uncommon serotypes is essential to identify and mitigate concealed risks to public health.

Salmonella spp. infections remain a major foodborne disease with global economic and health burdens (*1–3*). Current studies have predominantly targeted the epidemiology and molecular characteristics of prevalent serotypes, such as *Salmonella* Typhimurium, *Salmonella* Enteritidis, and *Salmonella* 4,[5],12:i:- (*4–5*), leaving gaps in the understanding of less prevalent serotypes. *Salmonella* Give, one of the rare serotypes of *Salmonella*, has caused hundreds of cases annually in Europe in recent years (the reported incidence is 0.02/100,000 to 0.08/100,000 from 2007 to 2024, https://atlas.ecdc.europa.eu/public/index.html). In the United States, *S.* Give is the 38th most prevalent serotype among *Salmonella* isolates in humans. Although *S.* Give is not the dominant serotype globally (*6*), its sporadic occurrence and localized outbreaks indicate its potential public health significance (*7–8*), warranting further investigation. *S.* Give ranks 14th among all serovars in China, with isolates recovered from both human and non-human sources (*9*); however, the prevalence of antimicrobial resistance (AMR), genetic characteristics, and transmission dynamics have rarely been reported. This study aimed to describe the genomic epidemiology and antimicrobial determinants of *S. Give* to provide a basic understanding of this serovar. This study used whole-genome-based approaches on national and global genomes to describe the genotypes, population structures, and AMR genes of *S. Give*. This study identified clonal expansion with the co-occurrence of an increasing prevalence of *qnrB19* and potential outbreaks in China.

METHODS

Data Source

From 2017 to 2024, 15,731 *Salmonella* genomes

were isolated and recorded in the National Pathogen Identification Network (CPIN) database. The whole-genome sequences and geographical data of 185 *S.* Give strains with geographical data, ranked 14th in the database. Most isolates (173/185) were recovered from the feces of patients with diarrhea, 10 from food sources, and 2 from unknown sources (Supplementary Figure S1, available https://weekly.chinacdc.cn/).

Genotyping and Antimicrobial Resistance Gene (ARG) Detection

Multilocus sequence typing (MLST) was performed using PubMLST (https://pubmlst.org/). The ARGs were determined by ResFinder 4.1.0 (https://genepi.food.dtu.dk/resfinder) with the screening criteria set as sequence identity ≥80% and coverage ≥60% to ensure the reliability of ARG annotations. Multidrug resistance (MDR) was defined as the concurrent carriage of ≥3 ARGs that individually belonged to different categories of antimicrobial agents. Plasmids were detected and compared via PlasmidFinder 2.1.0 (http://cge.cbs.dtu.dk/services/PlasmidFinder/) and NCBI BLASTn, respectively, and the resulting plasmids (≥95% identity, ≥90% coverage) were visualized linearly using Easyfig (https://mjsull.github.io/Easyfig/)

Phylogenetic Analysis

Quality control was conducted using Quast 5.0.2 (*10*) after retrieving the assembled genomic sequences from CPIN and EnteroBase, resulting in two genome subsets of *S.* Give: 185 domestic and 1,446 global genomes (https://enterobase.warwick.ac.uk/). Single-nucleotide polymorphisms (SNPs) in the core genome were determined with Snippy 4.4.5 (https://github.com/tseemann/snippy). The reference genome used in the phylogenetic tree was *S.* Give strain NCTC5778 (GCA_900477925.1), with a total length of 4,638,063 bp. SNP calling was performed using Snippy 4.4.5 (https://github.com/tseemann/snippy) with default parameters, resulting in about 7,000 core SNPs.

A maximum likelihood tree based on core-genome SNPs was constructed after removing recombinants using the Gubbins software 3.3.5 (https://github.com/nickjcroucher/gubbins) (*11*) and was presented using iTOL (https://itol.embl.de). Cluster analysis of plasmids carried by the strains was performed using the Average Nucleotide Identity (ANI) 1.34.

RESULTS

Sequence Type Distribution and Geographic Spread of *S.* Give in China

MLST of *S.* Give revealed that the sequence type ST516 was predominant (92.43%), followed by ST654 (5.9%), and three novel sequence types were identified in China (Supplementary Figure S1). Human-derived isolates constituted the majority of both ST516 (94.74%) and ST654 (90.91%) cases, whereas isolates from food sources were relatively rare (4.09% for ST516 and 9.09% for ST654; Supplementary Figure S1). ST516 was distributed across 24 provincial-level administrative divisions (PLADs), with a slightly higher prevalence in the eastern and southern regions than in the other regions. Specifically, the prevalence of ST516 in eastern China was 95.93%, which was higher than that in central (84.62%) and western (86.96%) China, with a prevalence of 94.26% exceeding that in northern China (88.89%). In contrast, ST654 was more frequently detected in central (12.5%) and western (13.04%) regions than in eastern China (2.46%; Figure 1A). Temporally, ST516 was first detected in eastern China and was subsequently identified in the central and western regions in this study (Figure 1A). ST654 was initially reported in 2021 (eastern region) with subsequent detections in 2023 (central and western regions) and 2024 (central region), demonstrating a progressive increase in the central region and a transient increase followed by a decline in the eastern and central regions (Figure 1A).

Quinolone Resistance and ARG Profiles of *S.* Give in China

Analysis of 185 *S.* Give isolates revealed 24 ARGs across nine categories. All isolates harbored the aminoglycoside resistance gene *aac(6')-Iaa* and the fluoroquinolone resistance-associated mutation *parC* p.T57S. Approximately 55.68% of the isolates carried the quinolone resistance gene, *qnrB19*, whereas other resistance genes were infrequent (<5%; Supplementary Table S1, available at https://weekly.chinacdc.cn/). ST516 exhibited the broadest ARG repertoire, with 14 ARGs present in >50% of the isolates (Figure 1B). In contrast, ST654 displayed limited diversity and prevalence of resistance genes, except for the universal presence of *parC* p.T57S and *aac(6')-Iaa* (both 100%; Figure 1B). The MDR rate was 3.51%, which was primarily associated with the presence of *parC* p.T57S, *dfrA14*, *floR*, and *sul3* and was exclusively observed in

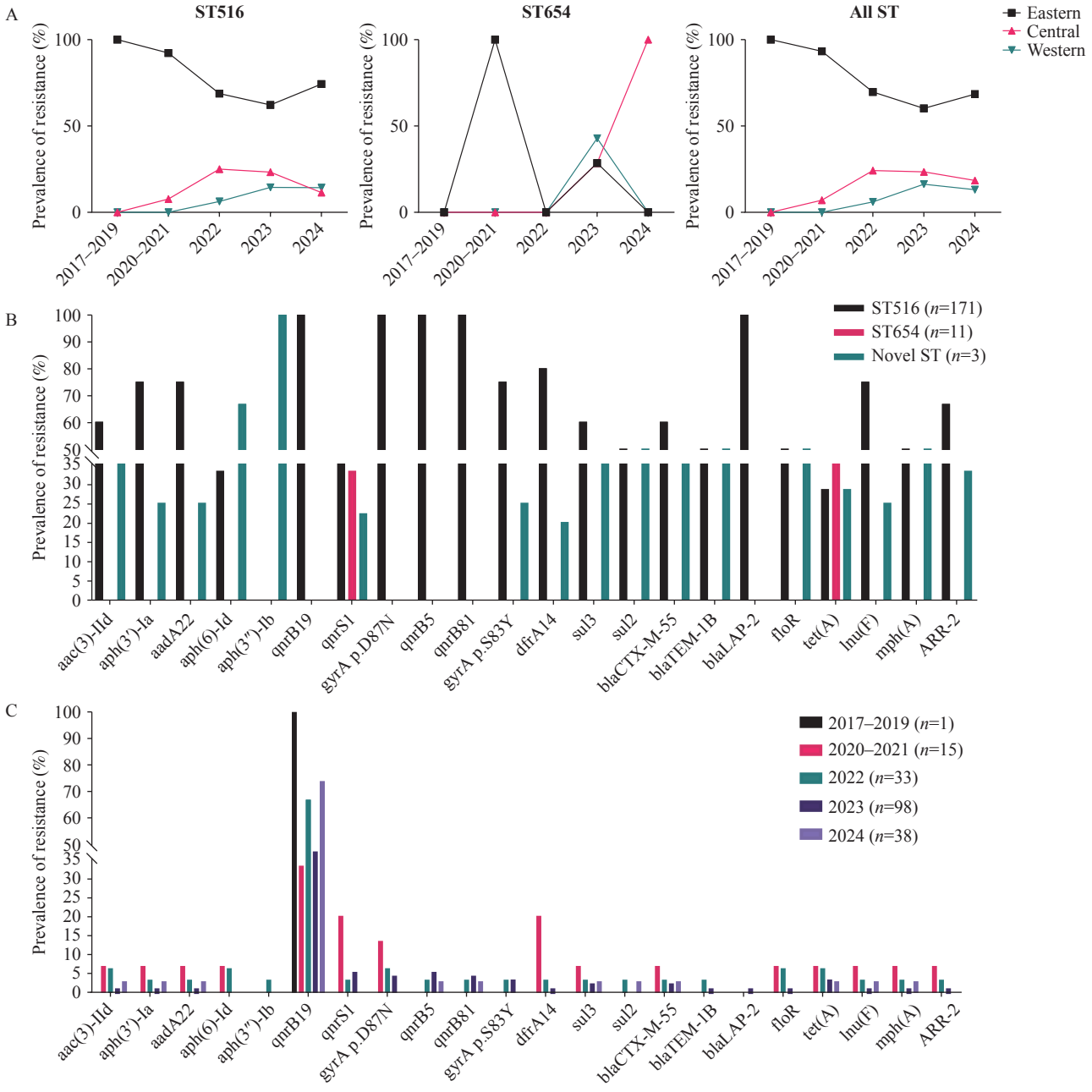

FIGURE 1. Dynamic distribution of STs and their associated ARGs. (A) shows the temporal trends of ST516, ST654, and all strains across the eastern, central, and western regions. (B) depicts the proportions of different resistance genes within various STs. (C) illustrates the proportions of different resistance genes throughout the years.
Abbreviation: ST=sequence type; ARG=antimicrobial resistance gene.

ST516. The extended-spectrum β-lactamase (ESBL) gene *bla*$_{\text{CTX-M-55}}$ was detected in five isolates from five PLADs. These isolates also harbored *sul3*, *qnrS1*, *aac(3)-IId*, *lnu(F)*, *ARR-2*, and *tet(A)*, which confer resistance to third-generation cephalosporins, sulfonamides, fluoroquinolones, aminoglycosides, lincosamides, and tetracyclines. Although the number of isolates varied across the years, a noticeable increase in *qnrB19* detection was observed in the later years of surveillance, whereas many other ARGs appeared stable or fluctuated at low levels (Figure 1C).

Clonal Expansion and Widespread Carriage of the *qnrB19* Gene, Especially Plasmid-mediated *qnrB19* Dissemination, in China

A phylogenetic tree based on core-genome SNPs

revealed that the 185 *S.* Give strains formed two lineages: A (11 strains) and B (174 strains). All isolates in lineage A were classified as ST654, whereas lineage B comprised ST516 and three novel sequence types. Lineage B was further subdivided into three sub-lineages (Figure 2). Sublineage 1 included 35 strains distributed across 12 PLADs in three regions over five years and was characterized by a broad spectrum of resistance genes up to 13 types; (Table 1), although the prevalence of each gene was low (2.86%–22.86%). Sublineage 2 (10 strains) was restricted to two PLADs in the eastern region over three years, with no resistance genes detected. Sublineage 3 represents the predominant clonal group (129/174; 74.14%), spanning all 24 PLADs from 2017 to 2024. This sublineage also harbored multiple resistance genes up to 13 types; (Table 1), with a notably higher carriage rate of *qnrB19* (79.84%) than that of other genes (0.78%–5.43%). Furthermore, 86.41% of *qnrB19*-positive strains in sublineage 3 carried the Col (pHAD28) plasmid (2.6kb) encoding *qnrB19* (Figure 2). In contrast, lineage A (ST654) contained only *tet(A)* and *qnrS1* (excluding the *parC* mutation and *aac(6')-Iaa*), each with a carriage rate of 27.27%. Temporal and geographic distributions of the three sublineages varied across PLADs and years. For example, in Shandong and Sichuan provinces, sublineage 1 predominated in 2021, but was supplanted by sublineage 3 in 2022 and 2023, respectively.

Six clusters of *S.* Give were detected in China. Two clusters, A and B, were located within lineage A. Cluster A comprised five ST654 strains differing by 2–3 SNPs (Figure 2), which were isolated from three cities (Yibin, Ningbo, and Jinhua) in May 2023, suggesting an interprovincial outbreak. Cluster B consisted of three closely related strains (0–3 SNP differences) detected in Xiangyang, Hubei Province, in 2024, which was consistent with a localized outbreak. Cluster C, within sublineage 1, comprised five strains differing by <5 SNPs and was identified in Guangdong Province. Cluster D, comprising nine strains with 0–5 SNPs differences, was found in Zhejiang Province, indicating another regional outbreak. Within sublineage 3, cluster E consisted of six *qnrB19*-negative strains (0–5 SNP differences) collected in Jiangxi Province (Figure 2), which were phylogenetically adjacent to *qnrB19*-positive strains and unique among the clusters, with all others carrying *qnrB19*. Additionally, Cluster F, comprising 30 closely related isolates differing by only 0–2 SNPs, was identified in the same sublineage (Figure 2).

ANI clustering analysis was performed on the Col(pHAD28) plasmids harboring 89 strains, grouping them into six clusters (A–F) (https://enterobase.warwick.ac.uk/). The intracluster similarity ranged from 97.29% to 100.00%. The sequence of the Col(pHAD28) plasmids (2,699 bp+) displayed high identity with 600 plasmids from 10 genera and 15 species. This indicates that small ColE1/Col440I-like plasmids (2.6–3.0 kb), carrying almost exclusively the *qnrB19* gene, are highly conserved and widely distributed across diverse bacterial species (*12*–*14*).

S. Give Exhibited Geographical and Source Clustering Worldwide, with a Potential Global Increase in *qnrB19*-harboring

Among the 1,631 global isolates of *S.* Give, five major STs were identified, of which ST516 was the most prevalent (45.62%), followed by ST654 (42.49%). ST654 was almost exclusively concentrated in the United States (82.70%), whereas ST516 was the predominant ST in all other countries, including China (Figure 3, and https://enterobase.warwick.ac.uk/). Additionally, ST2589, ST524, and ST2227 exhibited distinct regional distribution patterns; for example, ST2589 was mainly detected in Mexico (22 isolates, 22%), whereas ST524 was largely confined to the UK (27 strains, 34.2%).

The phylogenetic analyses revealed three global lineages (Figure 3). Lineage 1, dominated by ST516 (95.90%), is mainly distributed in Europe and Asia, with human-derived isolates being the primary source, followed by animal and food sources. Lineage 2 consisted mostly of ST516 (75.89%) and ST524 (17.32%), which exhibited a broad geographical range and balanced representation across different sources, with animal isolates being the most common. Lineage 3 was primarily composed of ST654 (91.18%), which is concentrated in North America, and over 70% of its isolates were from environmental sources. Chinese isolates were predominantly clustered in lineage 1, with only a scattered distribution in lineages 2 and 3. The phylogenetic reconstruction of 744 ST516 strains indicated a close genetic relationship between the Chinese isolates and UK food-derived strains (Supplementary Figure S3, available at https://weekly.chinacdc.cn/), suggesting a shared common ancestor and potential transnational transmission via the food

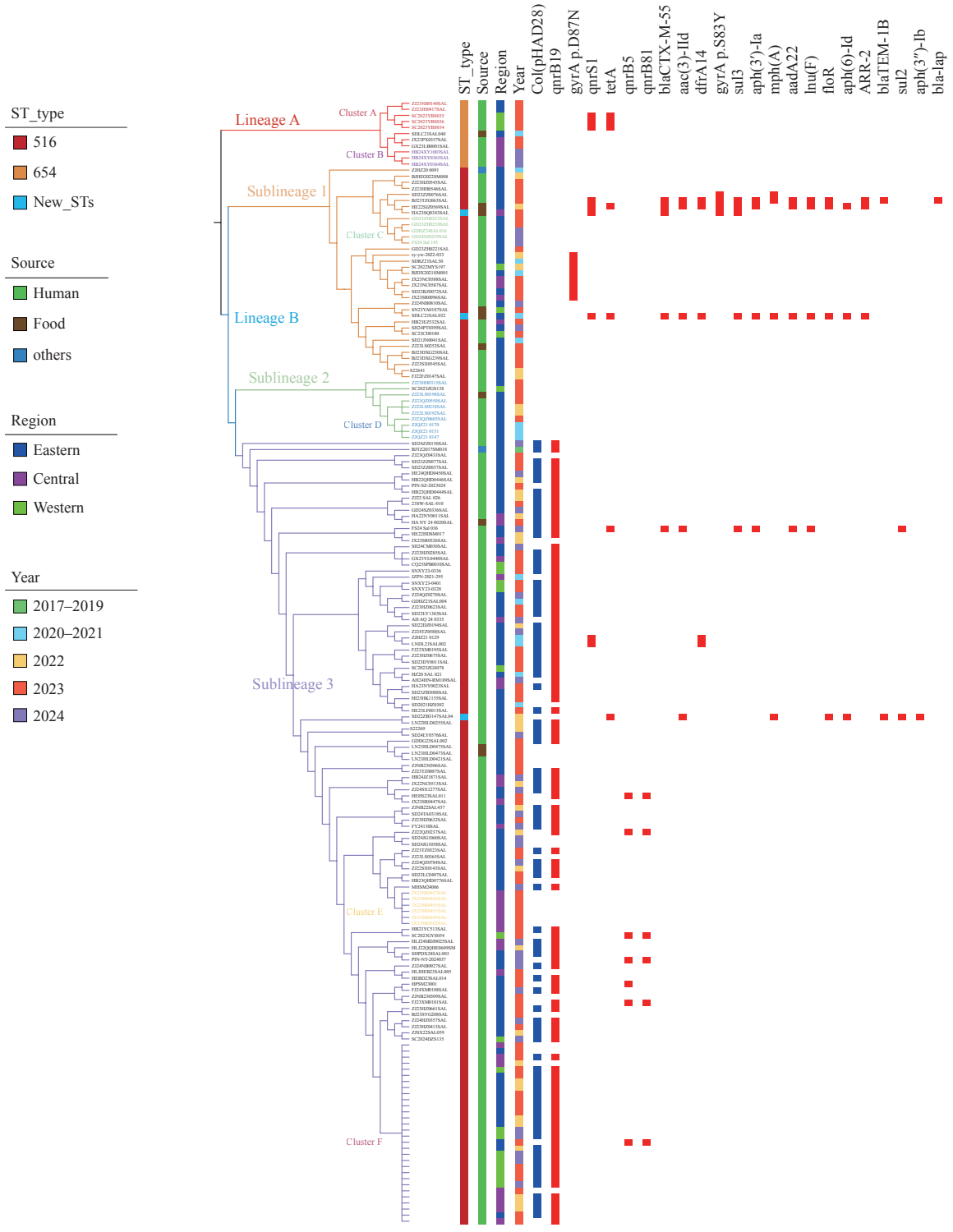

FIGURE 2. Phylogenetic tree of 185 *S.* Give isolates in China from 2017 to 2024 based on core-genome SNPs.
Note: The evolutionary tree is divided into two lineages: lineage A (red) and lineage B. Lineage B is further subdivided into three parts: sublineage 1 (yellow), sublineage 2 (blue), and sublineage 3 (purple).Six clusters coexist on the evolutionary tree: Cluster A (red), Cluster B (purple), Cluster C (green), Cluster D (blue), Cluster E (yellow), and Cluster F (blue-purple). The evolutionary tree is organized from the left to right layers as follows: STs (ST516, ST654, and three new STs), source (human, food and others), region (eastern, central, and western), year (2017-2019, 2020-2021, 2022, 2023, and 2024), and plasmid (Col(pHAD28)) and resistance genes (in order: *qnrB19, gyrA* p.D87N*, qnrS1, tetA, qnrB5, qnrB81, bla*$_{\text{CTX-M-55}}$*, aac(3)-IId, dfrA14, gyrA* p.S83Y*, sul3, aph(3')-Ia, mph(A), aadA22, lnu(F), floR, aph(6)-Id, ARR-2, bla*$_{\text{TEM-1B}}$*, sul2, aph(3'')-Ib, and bla-*$_{\text{LAP2}}$). Abbreviation: SNPs=single-nucleotide polymorphisms.

TABLE 1. The situation of antibiotic resistance gene carriage in different branches of the phylogenetic tree of 185 strains.

lineage		ARGs profile	Number of ARGs	Number of Strains
Lineage A		*qnrS1-tet(A)*	2	3
		gyrA p.S83Y	1	1
		No ARGs	–	6
	Sublineage 1	*gyrA* p.D87N	1	6
		gyrA p.S83Y	1	3
		mph(A)-gyrA p.S83Y	1	1
		qnrS1-sul3-blaCTX-M-55	2	1
		blaTEM-1B-floR-qnrS1-sul3-aac(3)-IId-mph(A)-dfrA14-aph(3')-Ia-blaCTX-M-55-ARR-2-aadA22-blaLAP-2-lnu(F)	3	1
		floR-qnrS1-sul3-aac(3)-IId-tet(A)-aph(6)-Id-dfrA14-aph(3')-Ia-blaCTX-M-55-ARR-2-aadA22-lnu(F)	13	1
		floR-qnrS1-sul3-aac(3)-IId-tet(A)-mph(A)-aph(6)-Id-dfrA14-aph(3')-Ia-blaCTX-M-55-ARR-2-aadA22-lnu(F)	12	1
		No ARGs	–	22
	Sublineage 2	No ARGs	–	10
Lineage B	Sublineage 3	*qnrB19*	1	90
		qnrB19-qnrB81-qnrB5	3	6
		qnrB19-qnrS1-dfrA14	3	2
		gyrA p.D87N	1	2
		qnrB19-gyrA p.D87N	2	2
		qnrB19-sul2-sul3-aac(3)-IId-tet(A)-aph(3')-Ia-blaCTX-M-55-aadA22-lnu(F)	9	1
		qnrB19-gyrA p.S83Y	2	1
		qnrB19-qnrB5	2	1
		blaTEM-1B-floR-sul2-aac(3)-IId-tet(A)-mph(A)-aph(6)-Id-aph(3'')-Ib	8	1
		No ARGs	–	23

chain.

Similar to the domestic strains, all global isolates carried the *aac(6')-Iaa* gene and *parC* p.T57S mutation, whereas only 8.95% of the isolates harbored the *qnrB19* gene. Among the *qnrB19*-positive isolates, most (70.55%) originated in China, followed by Nigeria (18%), France (6.87%), and the UK (6.25%). These isolates were predominantly assigned to ST516 and clustered in lineages 1 and 2, but were nearly absent in lineage 3 (Figure 3). Additionally, the source of *qnrB19* varied geographically. In China and Nigeria, *qnrB19* was almost exclusively detected in human isolates (100% of *qnrB19*-positive isolates from both countries were human-derived), whereas in the UK and France, *qnrB19* was detected more frequently in animal than human-derived isolates (Figure 3). Specifically, the detection rate of *qnrB19* in animal-derived isolates was 55.56% in the UK and 63.64% in France, compared with 27.78% and 36.36% in human-derived isolates from the UK and France, respectively (Figure 3). Notably, 95.21% of *qnrB19*-positive strains were recovered during the past decade, indicating a recent global increase in the spread of *qnrB19*-carrying *S.* Give. Furthermore, 129 of 146 *qnrB19* alleles were located on the Col(pHAD28) plasmid, of which 89 (68.99%) were detected in China (Figure 2, Figure 3 and Supplementary Table S1), suggesting the ongoing domestic circulation of this small mobilizable resistance plasmid in *S.* Give. Notably, among the global genomes, 22 environmental isolates (30.14% of all environmental samples) and 19 food isolates (26.03% of all food samples) harbored multiple resistance genes together with the chromosomal *gyrA* p.S83Y mutation (Figure 3, https://enterobase.warwick.ac.uk/), suggesting that MDR-associated determinants were present in both environmental- and food-associated *S.* Give populations.

DISCUSSION

This study provided a comprehensive analysis of the phylogenetic structure, spatiotemporal dissemination,

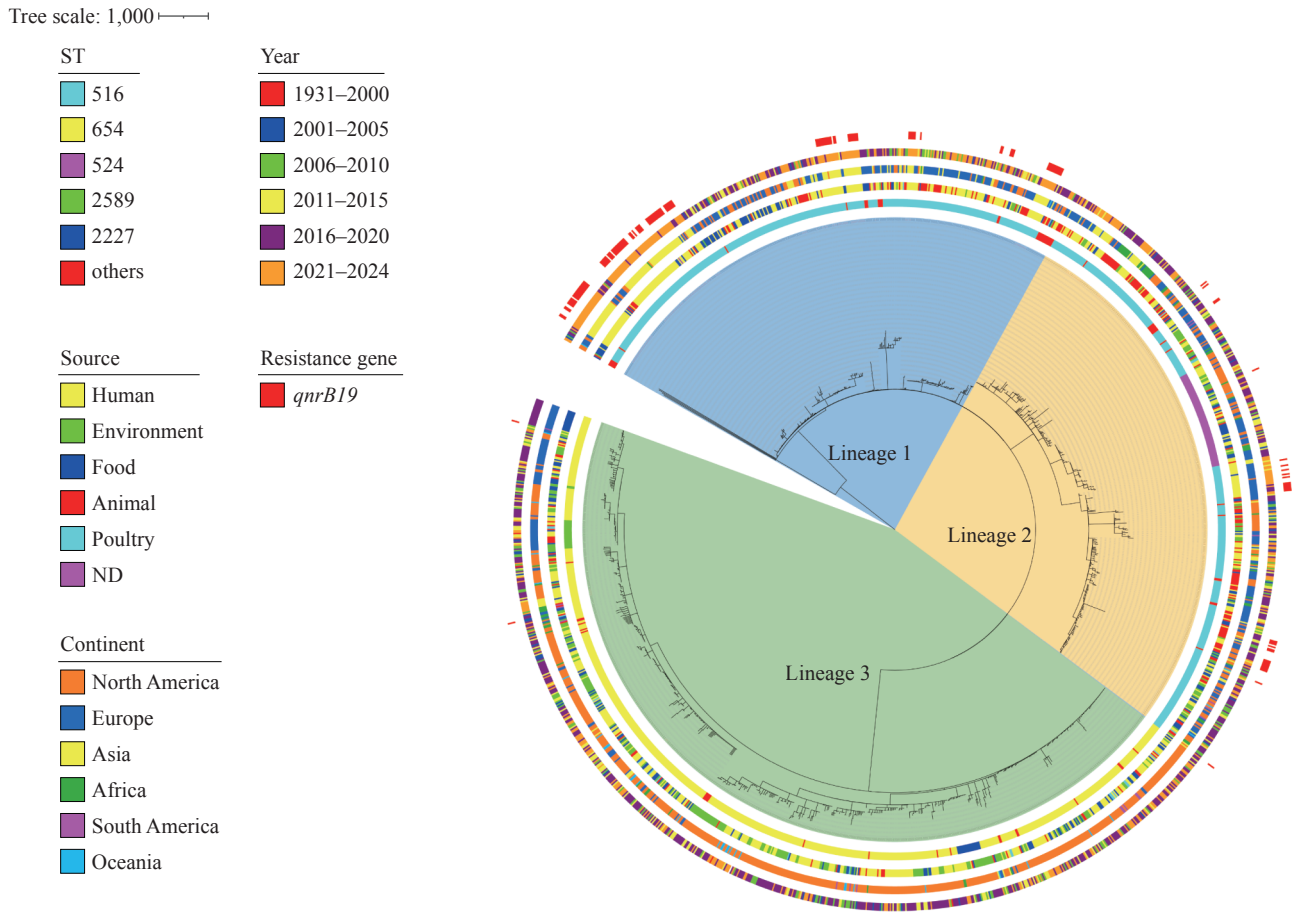

FIGURE 3. Phylogenetic tree of 1,631 global *S.* Give isolates from 1935 to 2024 based on core-genome SNPs.
Note: The evolutionary tree constructed on the basis of core genome multilocus sequence analysis is organized from the inner to outer layers as follows: Seven continents/regions (China, North America, Europe, Asia, Africa, South America, and Oceania); Sequence types (STs): Major STs including ST516, ST654, ST524, ST2589, ST2227, and other STs; Temporal distribution: Five time periods (1931–2000, 2001–2005, 2006–2010, 2011–2015, and 2016–2024); Source: Five categories (Human, Environment, Food, Animal, and Poultry). The phylogenetic tree is primarily divided into three lineages: lineage 1 (415 strains) with a blue background color, lineage 2 (456 strains) with a yellow background color, and lineage 3 (760 strains) with a green background color. Chinese strains are labeled in red and clustered within lineage 1 (139/185).
Abbreviation: SNP=single-nucleotide polymorphism; ST=sequence type.

and AMR profiles of *S.* Give in China. These findings reveal the high global genetic diversity of *S.* Give and identify the presence and increasing prevalence of an ST516 clone in China that is associated with the mobile fluoroquinolone resistance gene, *qnrB19*.

The majority of S. Give isolates in this study were pan-susceptible to antibiotics; however, there were several MDR isolates of ST516 in China. This genotype is characterized by various resistance genes, including those associated with chloramphenicol (*floR*), sulfonamide (*sul3*), cephalosporin ($bla_{\text{CTX-M-55}}$), and quinolone resistance (*qnrB19*, *qnrS*).

qnrB19 is widely distributed across diverse enterobacteria and is typically located on small plasmids such as IncQ, IncC, and Col (*15*). In the United States, approximately 95.4% of waterborne *S.* Enteritidis isolates carry the plasmid-mediated *qnrB19* (*16*). Similarly, in Poland, *qnrB19* has been identified as a key quinolone resistance gene that requires monitoring across multiple *Salmonella* serotypes (*17*). The plasmid Col(pHAD28) carrying *qnrB19* has been detected in *S.* Kentucky from poultry in Nigeria, including in environmental and clinical isolates from Ukraine and Bangkok (*18–20*), indicating its potential for dissemination across geographic regions and host species. In contrast to the predominant serotypes in China (*Salmonella* 4,[5],12:i:-), the prevalence of *qnrB19* is <1%, with *qnrS1* being more frequently detected (*4*). Studies have shown that *qnrB19* alone can increase the minimum inhibitory concentration (MIC) of ciprofloxacin 10-fold and moxifloxacin 8-fold *in vitro* (*21*). When combined with the *gyrA*

mutation S83F/D87N, *qnrB19* synergistically enhances fluoroquinolone resistance by 2-2.5 fold (*22*). However, the interaction between *qnrB19* and *parC* p.T57S remains unclear and requires further investigation.

Col(pHAD28) is non-self-transmissible (*23*), and its mobilization depends on conjugative plasmids such as IncHI2 or IncF, which provide a type IV secretion system (T4SS) for horizontal transfer, which may explain the relatively low *qnrB19* prevalence in dominant Chinese *Salmonella* serotypes. However, recent surveillance data have shown an upward trend in *qnrB19* carriage among *S.* Typhimurium and *Salmonella* 4,[5],12:i:- in China, suggesting a potential increase in quinolone resistance mediated by this gene. A global genomic analysis of 47,452 *Salmonella* isolates (1905–2020) revealed a low overall prevalence of *qnrB19*: 0.43% for *qnrB19* alone and 0.87% for *qnrB19-parC* p.T57S combination (*24*). A review of 22 publications involving 468 strains revealed the widespread distribution of *qnrB19* across 49 *Salmonella* serotypes in nine countries (339 strains from the Americas, 63 from Europe, and 67 from Africa, *25-28*). These findings are consistent with the data on *qnrB19* in Asia (excluding China), where only 33 human-derived strains have been identified (primarily from Brazil and Nigeria). Except for one strain lacking the ColE-like replicon, all *qnrB19*-positive strains carried Col(pHAD28), indicating a strong association between *qnrB19* and this plasmid type in *Salmonella*.

Epidemiological data have highlighted the public health significance of *S.* Give in China. *S.* Give accounts for 1.18% of human-derived *Salmonella* isolates (ranking 13th); based on the national salmonellosis incidence of 1,295.59/100,000 *(29)*, the estimated burden of *S.* Give is approximately 15/100,000, substantially higher than the incidence of typhoid and paratyphoid fevers (≈0.5/100,000). Additionally, *S.* Give genomes constitute 0.17%–0.27% of the global *Salmonella* genomic database submissions (as of June 17, 2023), suggesting that its incidence or disease burden in China exceeds the global average and is higher than that in developed regions such as Europe and the United States. Combined with the emergence and clonal expansion of genotype ST516 linked to the increasing prevalence of *qnrB19*, this highlights public health threats.

This study had several limitations. Chinese strains were primarily derived from human sources, which may have introduced a selection bias. Second, the lack of clinical metadata (e.g., disease outcomes, exposure history, and travel history) limits insights into the factors influencing resistance patterns and transmission.

In conclusion, to our knowledge, this is the first genetic analysis of *S.* Give. This study reveals important information about serovar AMR and population structure. The results revealed that the number of ARGs harbored by *S.* Give was relatively limited; however, *qnrB19* prevalence was high among both domestic and international isolates. These findings underscore the necessity for continuous and robust genomic surveillance to detect and mitigate concealed risks to public health.

Conflicts of interest: No conflict of interests.

Acknowledgments: We gratefully acknowledge all staff from the relevant provinces for their participation in *Salmonella* isolation.

Ethical statement: This study does not involve human subjects, animals, or any clinical research. Therefore, ethical approval from an ethics committee is not required.

doi: 10.46234/ccdcw2026.037

[#] Corresponding author: Meiying Yan, yanmeiying@icdc.cn.

[1] National Key Laboratory of Intelligent Tracking and Forecasting for Infectious Diseases, National Institute for Communicable Disease Control and Prevention, Chinese Center for Disease Control and Prevention.

Accepted: February 21, 2026
Issued: February 27, 2026

REFERENCES

1. Popa GL, Papa MI. *Salmonella* spp. infection—a continuous threat worldwide. Germs 2021;11(1):88 – 96. https://doi.org/10.18683/germs.2021.1244.
2. Harrison OL, Rensing S, Jones CK, Trinetta V. *Salmonella enterica* 4,[5],12:i:-, an emerging threat for the swine feed and pork production industry. J Food Prot 2022;85(4):660 – 3. https://doi.org/10.4315/JFP-21-400.
3. Teklemariam AD, Al-Hindi RR, Albiheyri RS, Alharbi MG, Alghamdi MA, Filimban AAR, et al. Human salmonellosis: a continuous global threat in the farm-to-fork food safety continuum. Foods 2023;12(9):1756. https://doi.org/10.3390/foods12091756.
4. Sun HY, Cui ZG, Du XL, Fan FX, Sun BW, Diao BW, et al. Prevalence of *Salmonella enterica* serotype 4,[5],12:i:- from human sources: antimicrobial resistance, genotypic diversity and emergence of carbapenem resistance - China, 2017-2023. China CDC Wkly 2025;7(24):821 – 30. https://doi.org/10.46234/ccdcw2025.134.
5. Moreau MR, Edison LK, Ivanov YV, Wijetunge DSS, Hewage EMKK, Linder JE, et al. Comparative patho-genomics of *Salmonella enterica* serovar enteritidis reveal potential host-specific virulence factors. Pathogens 2025;14(2):128. https://doi.org/10.3390/pathogens14020128.

6. Wang YN, Xu XB, Jia SL, Qu MQ, Pei YH, Qiu SF, et al. A global atlas and drivers of antimicrobial resistance in *Salmonella* during 1900-2023. Nat Commun 2025;16(1):4611. https://doi.org/10.1038/s41467-025-59758-3.
7. Peresi JTM, De Almeida IAZC, De Carvalho Teixeira IS, De Lima E Silva SI, Graciano RAS, Tiba-Casas MR. High rates of *Salmonella* contamination in raw kibbe from commercial establishments: predominance of *Salmonella* give. Int J Environ Health Res 2021;31(6):626 – 35. https://doi.org/10.1080/09603123.2019.1679356.
8. Flórez NY, Arévalo SA, Rodríguez EC, Guerrero J, Valverde KP, Díaz PL, et al. An outbreak of *Salmonella enterica* subsp. *enterica* serovar Give associated with foodborne illness in the department of Vichada, Colombia, 2015. Biomedica 2021;41(1):41-51. http://dx.doi.org/10.7705/biomedica.5206.
9. Wang YN, Liu Y, Lyu N, Li ZY, Ma SF, Cao DM, et al. The temporal dynamics of antimicrobial-resistant *Salmonella enterica* and predominant serovars in China. Natl Sci Rev 2022;10(3):nwac269. https://doi.org/10.1093/nsr/nwac269.
10. Gurevich A, Saveliev V, Vyahhi N, Tesler G. QUAST: quality assessment tool for genome assemblies. Bioinformatics 2013;29(8):1072 – 5. https://doi.org/10.1093/bioinformatics/btt086.
11. Croucher NJ, Page AJ, Connor TR, Delaney AJ, Keane JA, Bentley SD, et al. Rapid phylogenetic analysis of large samples of recombinant bacterial whole genome sequences using Gubbins. Nucleic Acids Res 2015;43(3):e15. https://doi.org/10.1093/nar/gku1196.
12. Peirano G, Matsumara Y, Pitout JDD. Mobile genetic elements of global *Escherichia coli* ST131 clades with carbapenemases. Eur J Clin Microbiol Infect Dis 2025;44(9):2119 – 28. https://doi.org/10.1007/s10096-025-05187-5.
13. Argueta F, Tatarenkov A, Mota-Bravo L. Multiple copies of a *qnrB19* gene are carried by tandem repeats of an IS*26* composite transposon in an *Escherichia coli* plasmid. Microbiol Resour Announc 2022;11(12):e00661 – 22. https://doi.org/10.1128/mra.00661-22.
14. Seriki AT, Obi C, Olashile AA, Essiet UU, Akingboye DW, Ajayi A, et al. Genomic analysis of multidrug resistant *Enterobacter hormaechei* strain AH1-NIMR isolated from a neonate with sepsis in Lagos, Nigeria. Infect Chemother 2025;57(2):316 – 20. https://doi.org/10.3947/ic.2025.0040.
15. Pallecchi L, Riccobono E, Sennati S, Mantella A, Bartalesi F, Trigoso C, et al. Characterization of small ColE-like plasmids mediating widespread dissemination of the *qnrB19* gene in commensal enterobacteria. Antimicrob Agents Chemother 2010;54(2):678 – 82. https://doi.org/10.1128/AAC.01160-09.
16. Monte DFM, de Lima Rocha AD, Lemos MLP, de Lima LA, Cabrera JM, da Silva NJ, et al. High prevalence of plasmid-mediated quinolone resistance in *Salmonella enterica* serovars isolated from surface water. Environ Microbiol 2025;27(7):e70140. https://doi.org/10.1111/1462-2920.70140.
17. Piekarska K, Wołkowicz T, Zacharczuk K, Stepuch A, Gierczyński R. The mechanisms involved in the fluoroquinolone resistance of *Salmonella enterica* strains isolated from humans in Poland, 2018-2019: the prediction of antimicrobial genes by in silico whole-genome sequencing. Pathogens 2023;12(2):193. https://doi.org/10.3390/pathogens12020193.
18. Jibril AH, Okeke IN, Dalsgaard A, Menéndez VG, Olsen JE. Genomic analysis of antimicrobial resistance and resistance plasmids in *Salmonella* serovars from poultry in Nigeria. Antibiotics (Basel) 2021;10(2):99. https://doi.org/10.3390/antibiotics10020099.
19. Stein C, Zechel M, Spott R, Pletz MW, Kipp F. Multidrug-resistant isolates from Ukrainian patients in a German health facility: a genomic surveillance study focusing on antimicrobial resistance and bacterial relatedness. Infection 2023;51(6):1731 – 8. https://doi.org/10.1007/s15010-023-02061-4.
20. Toyting J, Nuanmuang N, Utrarachkij F, Supha N, Thongpanich Y, Leekitcharoenphon P, et al. Genomic analysis of *Salmonella* isolated from canal water in Bangkok, Thailand. Microbiol Spectr 2024;12(5):e04216 – 23. https://doi.org/10.1128/spectrum.04216-23.
21. Suwanthada P, Kongsoi S, Jayaweera S, Akapelwa ML, Thapa J, Nakajima C, et al. Interplay between amino acid substitution in GyrA and QnrB19: elevating fluoroquinolone resistance in *Salmonella* typhimurium. ACS Infect Dis 2024;10(8):2785 – 94. https://doi.org/10.1021/acsinfecdis.4c00150.
22. Allou N, Cambau E, Massias L, Chau F, Fantin B. Impact of low-level resistance to fluoroquinolones due to *qnrA1* and *qnrS1* genes or a *gyrA* mutation on ciprofloxacin bactericidal activity in a murine model of *Escherichia coli* urinary tract infection. Antimicrob Agents Chemother 2009;53(10):4292 – 7. https://doi.org/10.1128/AAC.01664-08.
23. Mathers AJ, Peirano G, Pitout JDD. The role of epidemic resistance plasmids and international high-risk clones in the spread of multidrug-resistant *Enterobacteriaceae*. Clin Microbiol Rev 2015;28(3):565 – 91. https://doi.org/10.1128/CMR.00116-14.
24. Nuanmuang N, Leekitcharoenphon P, Njage PMK, Gmeiner A, Aarestrup FM. An overview of antimicrobial resistance profiles of publicly available *Salmonella* genomes with sufficient quality and metadata. Foodborne Pathog Dis 2023;20(9):405 – 13. https://doi.org/10.1089/fpd.2022.0080.
25. Braga PRC, dos Santos CA, de Jesus Bertani AM, Vieira T, Amarante AF, Reis AD, et al. Detection and genomic characterization of a multidrug-resistant *Salmonella* Newport co-harbouring bla_{CMY-2}, *qnrB19* and *mcr-9* from the diarrheic faeces of a foal. J Glob Antimicrob Resist 2023;35:198 – 201. https://doi.org/10.1016/j.jgar.2023.09.019.
26. Corradini C, De Bene AF, Russini V, Carfora V, Alba P, Cordaro G, et al. Detection of *Salmonella* reservoirs in birds of prey hosted in an Italian wildlife Centre: molecular and antimicrobial resistance characterisation. Microorganisms 2024;12(6):1169. https://doi.org/10.3390/microorganisms12061169.
27. Chen Z, Delgado Suárez EJ, Bonelli RR, Oliveira CJB, Moreno-Switt AI, Adell AD, et al. Exploring the genomic and antimicrobial resistance tapestry: comparative insights into *Salmonella enterica* serotypes Agona, Braenderup, Muenchen, and Panama in Latin American surface waters. Microbiol Spectr 2025;13(2):e01706 – 24. https://doi.org/10.1128/spectrum.01706-24.
28. Aworh MK, Nilsson P, Egyir B, Owusu FA, Hendriksen RS. Rare serovars of non-typhoidal *Salmonella enterica* isolated from humans, beef cattle and abattoir environments in Nigeria. PLoS One 2024;19(1):e0296971. https://doi.org/10.1371/journal.pone.0296971.
29. Fan PH, Han HH, Liu JK, Ma XC, Zhang RH, Liu H, et al. Community incidence estimates of five pathogens based on foodborne diseases active surveillance — China, 2023. China CDC Wkly 2024;6(24):574 – 9. https://doi.org/10.46234/ccdcw2024.112.

SUPPLEMENTARY MATERIAL

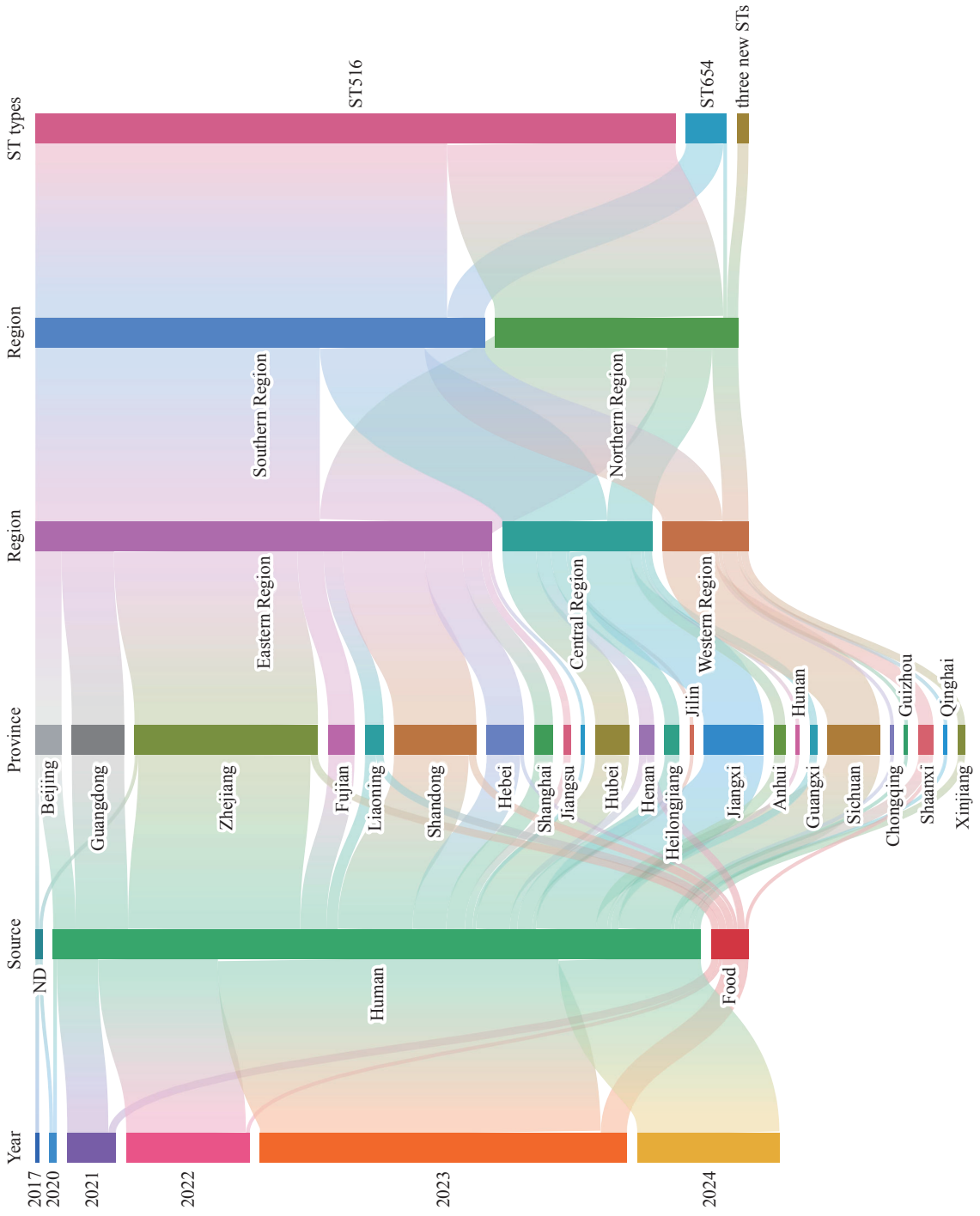

SUPPLEMENTARY FIGURE S1. Distribution of 185 S.Give strains collected in China between 2017 and 2024.
Note: From left to right: the isolation year, source, PLAD, region, and ST.
Abbreviation: PLAD=provincial-level administrative division; ST=sequence type.

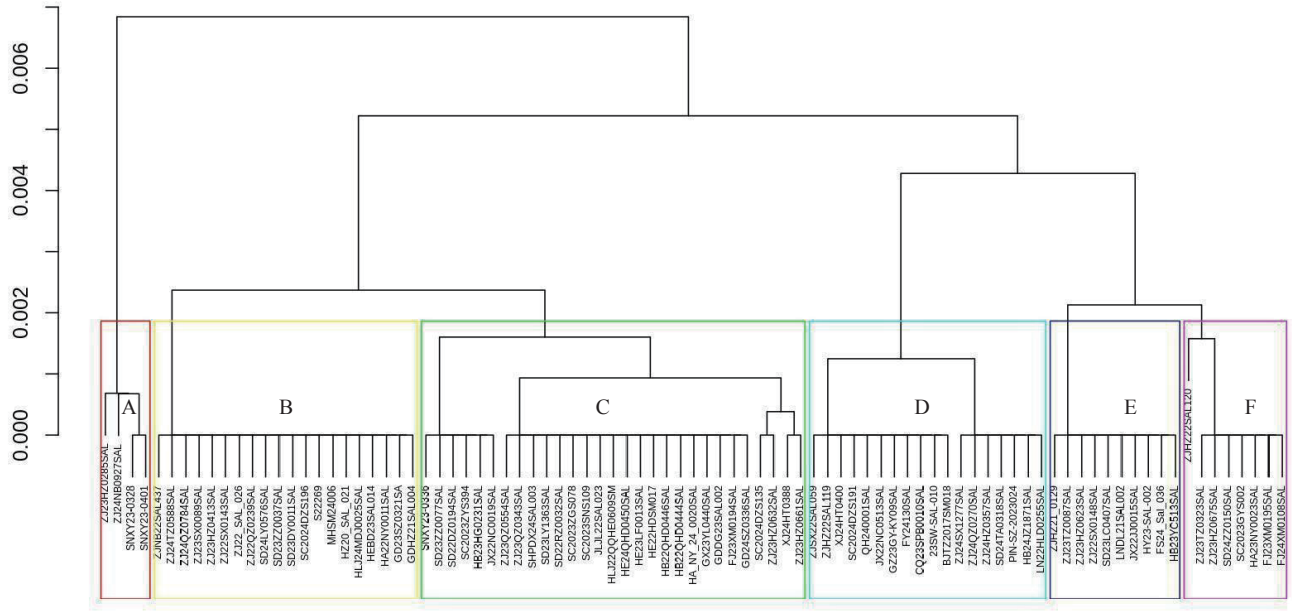

SUPPLEMENTARY FIGURE S2. ANI clustering analysis of the Col(pHAD28)plasmid carried by 89 strains.
Note: There are six clusters in sequence, denoted by A (red), B (yellow), C (green), D (blue), E (purple), and F (magenta).

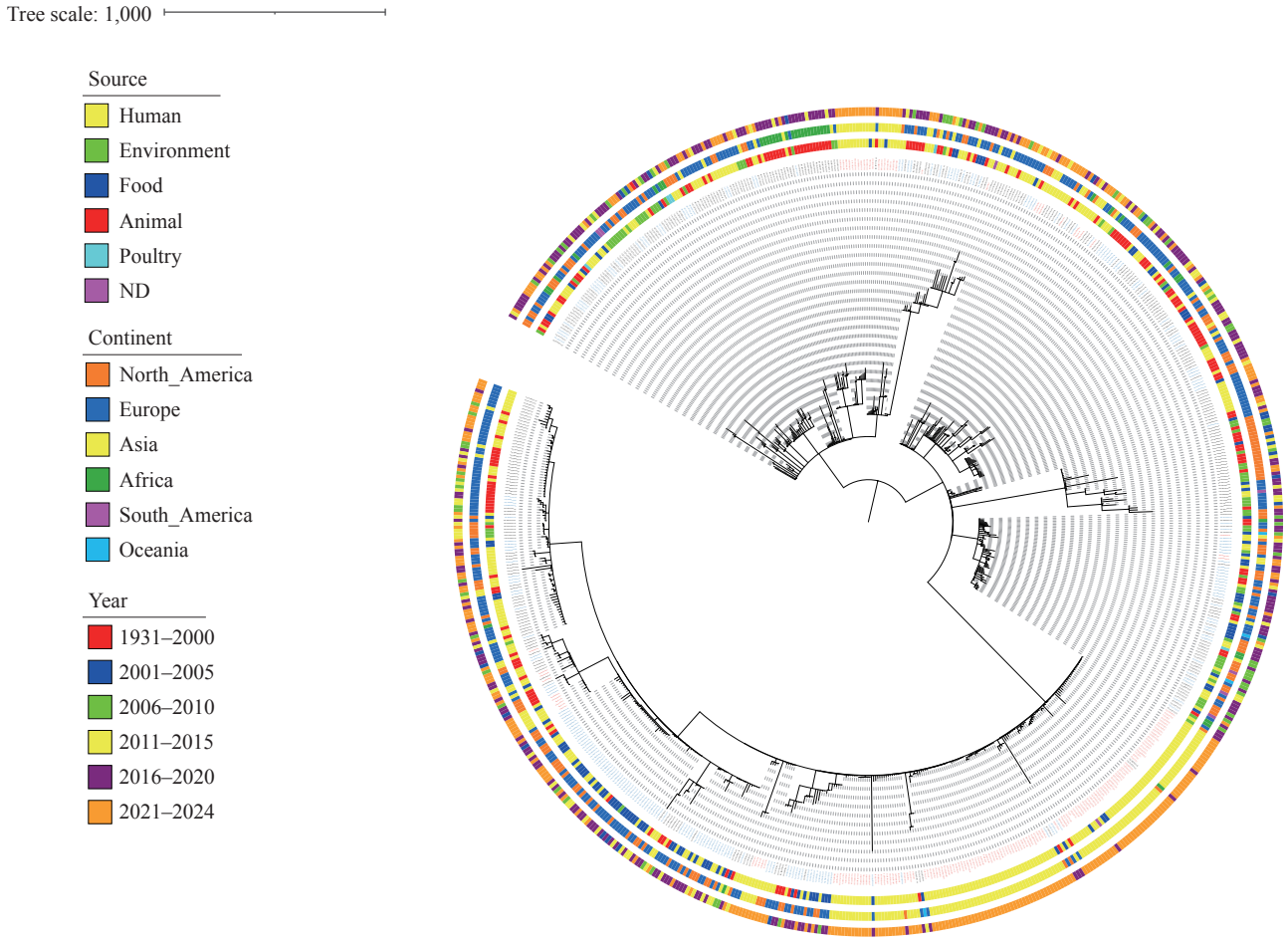

SUPPLEMENTARY FIGURE S3. Phylogenetic tree of 744 global ST516 S.Give isolates from 2000 to 2024 based on core-genome SNPs.

Note: The evolutionary tree constructed on core-genome SNPs is organized from the inner to outer layers as follows: source, continent, and year. Strains originating from China are labeled in red, and strains from the UK are labeled in blue. Abbreviation: SNP=single-nucleotide polymorphism.

SUPPLEMENTARY TABLE S1. The number of antibiotic resistance genes carried by 185 strains.

Classes of ARGs	Genotypes (*n*)	Percentage	ARGs	Number (%)
Aminoglycosides	6	100%	*aac(6')-Iaa*	185 (100)
			aac(3)-IId	5 (2.70)
			aph(3')-Ia	4 (2.16)
			aadA22	4 (2.16)
			aph(6)-Id	3 (1.62)
			aph(3'')-Ib	1 (0.54)
Quinolones	7	100%	*parC* p.T57S	185 (100)
			qnrB19	103 (55.68)
			qnrS1	9 (4.86)
			gyrA p.D87N	8 (4.32)
			qnrB5	7 (3.78)
			qnrB81	6 (3.24)
			gyrA p.S83Y	4 (2.16)
Folate Pathway Antagonists	3	4.30%	*dfrA14*	5 (2.70)
			sul3	5 (2.70)
			sul2	2 (1.08)
β-Lactams	3	3.24%	$bla_{CTX-M-55}$	5 (2.70)
			bla_{TEM-1B}	2 (1.08)
			bla_{LAP-2}	1 (0.54)
Chloramphenicol	1	2.16%	*floR*	4 (2.16)
Tetracyclines	1	3.78%	*tet(A)*	7 (3.78)
Lincosamides	1	2.16%	*lnu(F)*	4 (2.16)
Macrolides	1	2.16%	*mph(A)*	4 (2.16)
Rifamycins	1	1.62%	*ARR-2*	3 (1.62)

Preplanned Studies

Genomic Characterization of *Clostridium botulinum* Isolates from Soil and Soybean Samples in High-Incidence Regions — Xinjiang, Inner Mongolia, and Qinghai PLADs, China, 2024

Yongsi Zhan[1,2]; Xin Ma[3]; Xuebin Guo[4]; Meng Zhang[5]; Chunxia Cui[6]; Weiwei Li[2]; Shaofei Yan[2]; Shenghui Cui[7]; Xingfen Yang[1,#]; Yunchang Guo[1,2,#]

Summary

What is already known about this topic?

Foodborne botulism is prevalent in northwestern China, linked to traditional homemade foods. Recently, some cases have been linked to commercial vacuum-packaged ready-to-eat meat products. Soil is a potential contamination source, yet genomic information on environmental isolates from high-incidence regions remains scarce.

What is added by this report?

This study presents the first genomic characterization of 23 *C. botulinum* isolates obtained from soil and soybean samples in Northwest China. Four botulinum neurotoxin subtypes, A5(B3), B2, B3, and B4, were identified, each demonstrating notable geographic and metabolic diversity. Subtype-specific genomic adaptations, transposase insertions, and an incomplete prophage carrying *bont* in one isolate were observed, suggesting historical horizontal gene transfer.

What are the implications for public health practice?

Soils in high-incidence regions may act as persistent reservoirs of *C. botulinum*, emphasizing the need for targeted evidence-based public health interventions. Strengthening hygiene and sanitation practices during food processing, along with enhanced surveillance of both traditional and commercial food products, are essential to prevent future foodborne botulism outbreaks in endemic regions.

ABSTRACT

Introduction: *Clostridium botulinum* (*C. botulinum*) produces botulinum neurotoxins (BoNTs), the causative agents of botulism, a severe neuroparalytic disease prevalent in northwest China. Recent foodborne botulism outbreaks linked to commercially produced, vacuum-packaged, ready-to-eat foods were traced to raw meat contaminated with *C. botulinum* spores originating from soil, highlighting an emerging public health concern related to environmental reservoirs. However, genomic information on environmental isolates from high-incidence regions remains limited.

Methods: A total of 23 *C. botulinum* strains isolated from soil and soybean samples in northwest China were sequenced in 2024. Genomes were analyzed for plasmids, prophages, antibiotic resistance genes, virulence factors, and *bont*. Evolutionary relationships and adaptive features were investigated via phylogenetic and functional analyses.

Results: The 23 isolates were classified into four BoNT subtypes [A5(B3), B2, B3, B4] and clustered according to subtype and geographic origin. Isolates from Qinghai formed distinct branches. Functional annotation revealed subtype-specific metabolic variations, particularly in carbohydrate metabolism. Although all isolates contained conserved *bont* clusters, some exhibited transposase insertions. One subtype A5(B3) isolate harbored *bont* within an incomplete prophage.

Conclusion: These preliminary insights into environmental *C. botulinum* virulence, ecological adaptation, and evolutionary characteristics in northwest China provide a foundation for targeted surveillance and the development of preventive strategies against botulism in endemic regions.

Clostridium botulinum (*C. botulinum*) is a Gram-positive, spore-forming, and anaerobic bacillus that is ubiquitously distributed in soils, aquatic sediments, and animal feces, posing a potential risk for foodborne and environmental exposure. Botulism is a severe neuroparalytic disease caused by botulinum neurotoxin (BoNT) produced by *C. botulinum*. BoNTs are among

the most potent biological toxins and are classified into serotypes A–G, with types A, B, E, and F primarily associated with human disease (*1*).

In China, foodborne botulism (FB) exhibits a distinct geographical distribution, with a higher prevalence in northwestern provincial-level administrative divisions (PLADs) such as Xinjiang, Inner Mongolia, and Qinghai. Traditional dietary habits and local environmental conditions promote *C. botulinum* proliferation, and outbreaks are frequently associated with consumption of homemade fermented soybean products and dried meat contaminated with soil-derived spores (*2*–*4*). Additionally, recent FB outbreaks linked to commercial vacuum-packaged ready-to-eat foods were likely caused by contamination of raw meat with *C. botulinum* spores in soil, highlighting an emerging public health concern associated with environmental reservoirs (*5*–*6*). Most previous genomic studies focused on clinical or food isolates, whereas data on environmental isolates from high-incidence regions in China are scarce.

Here, we sequenced 23 *C. botulinum* isolates from soil and soybean samples from high-incidence regions in Northwest China and compared their genetic diversity, evolutionary dynamics, and virulence potential of reservoirs linked to human diseases. This study is critical for assessing public health risks and tailoring region-specific preventive strategies.

Twenty-three *C. botulinum* isolates were collected from Xinjiang (13 isolates, including 11 from soil and two from soybean samples), Inner Mongolia (8 isolates from soil), and Qinghai PLADs (2 isolates from soil) in 2024 (Supplementary Table S1, available at https://weekly.chinacdc.cn/). Genomic DNA was extracted using a Genomic DNA Purification Kit (Promega, Madison, WI, USA). Sequencing was performed by Beijing Novogene Bioinformatics Technology Co., Ltd. (Beijing, China) on an Illumina HiSeq platform (San Diego, CA, USA; 150-bp paired-end; 100× coverage depth). The quality of raw reads was assessed using FastQC (version 0.11.9). Clean reads were assembled *de novo* using SPAdes (version 4.1.0). Assembly quality was evaluated using QUAST (version 5.3.0; Algorithmic Biology Lab, St. Petersburg, Russia). Genome annotation was performed using Prokka (version 1.14.6; University of Melbourne, Melbourne, Australia). Plasmid sequences were identified using PlasmidFinder. A phylogenetic tree of *bont* was constructed using the neighbor-joining method in MEGA (version 11.0; Pennsylvania State University, State College, PA, USA), incorporating sequences from the isolates in this study and representative reference strains of subtypes A and B retrieved from GenBank (Supplementary Table S2, available at https://weekly.chinacdc.cn/). Core genome single-nucleotide polymorphisms (cgSNPs) were identified using Snippy (version 4.6.0; University of Melbourne, Melbourne, Australia). A maximum likelihood tree was generated using FastTree (version 2.1.10, San Diego, CA, USA) on the Galaxy platform (*7*). Sequence types were assigned using the PubMLST database. Phylogenetic trees and figures were generated and visualized using the ChiPlot web server (*8*). Predicted proteins were functionally annotated using the Clusters of Orthologous Genes (COG; https://ngdc.cncb.ac.cn/databasecommons/database/id/37) database, and principal component analysis of the COG category distributions was performed using R (version 4.4.0; The R Project for Statistical Computing, Vienna, Austria). Virulence genes in the Virulence Factor Database (https://www.mgc.ac.cn/VFs/) were identified using BLASTn. Antibiotic-resistance genes were detected using The Comprehensive Antibiotic Resistance Database (https://card.mcmaster.ca/). The 10-kb genomic regions flanking *bont* were compared using Easyfig (version 2.2.5, Brisbane, Australia). Prophage regions were predicted using the PHASTER web server.

The genomes of 23 isolates sequenced and assembled *de novo* showed sizes of 3.79–4.23 Mb and GC contents of 27.2%–28.3% (Supplementary Table S3, available at https://weekly.chinacdc.cn/). PlasmidFinder revealed no plasmids. Phylogenetic analyses based on *bont* genes, cgSNPs, and multilocus sequence typing consistently revealed that the 23 isolates clustered primarily according to subtype and sequence type. This included nine subtype A5(B3) and three subtype B3 isolates from Xinjiang; eight subtype B2 isolates from Inner Mongolia and one from Xinjiang; and two subtype B4 isolates from Qinghai (Figure 1). Isolates from Xinjiang and Inner Mongolia formed a closely related genetic cluster (Group I), whereas Qinghai isolates constituted a distinct phylogenetic branch (Group II). Notably, isolates FZSY033106030013 [A5(B3)], FZSY033106030017 (B2), and FZSY033106030015 (B3) exhibited unique sequence types and greater genetic distances from others within the same subtype, suggesting microevolution or distinct ancestral origins.

Functional annotation assigned the predicted proteins to 23 categories. Excluding proteins with

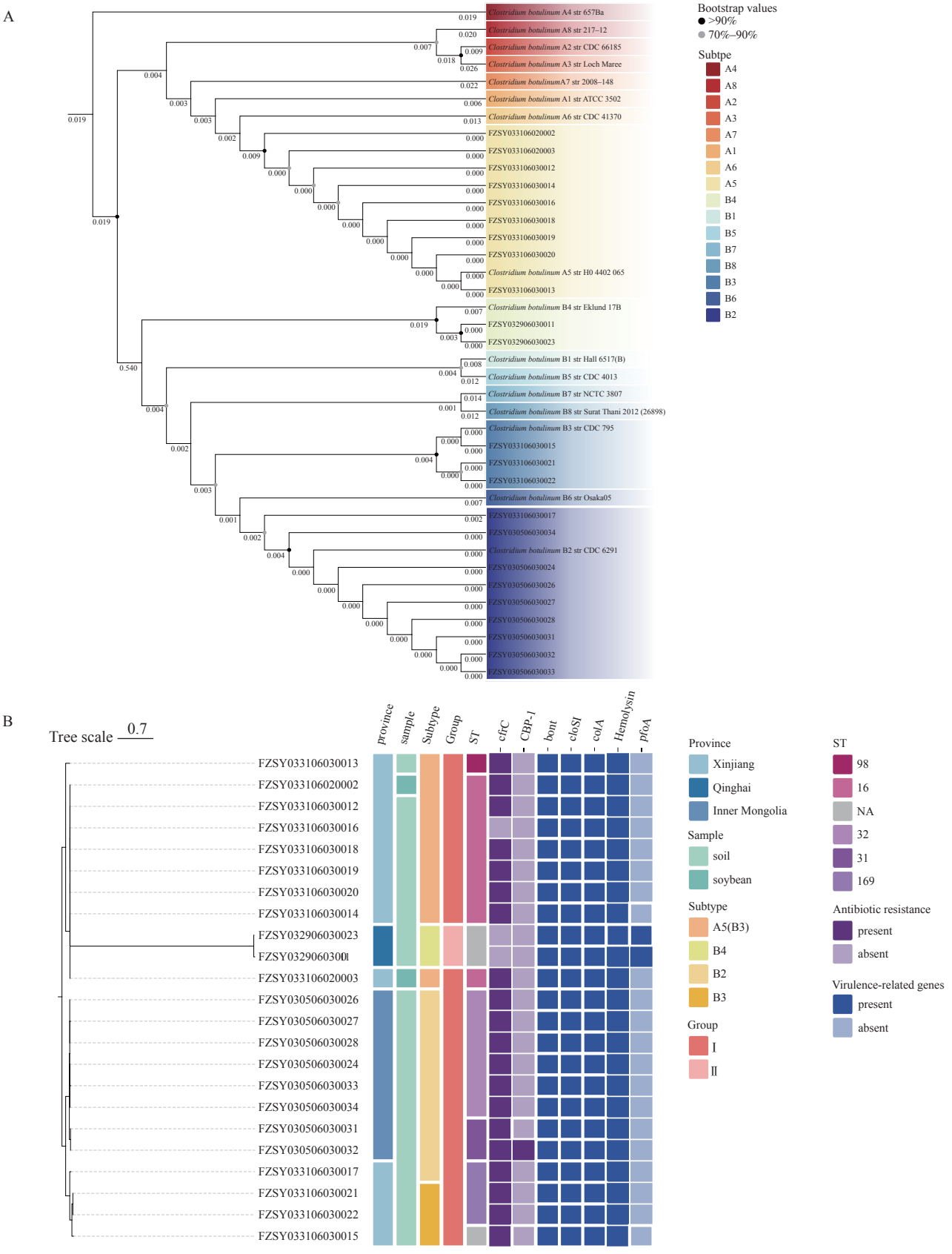
A
Clostridium botulinum A4 str 657Ba
Clostridium botulinum A8 str 217–12
Clostridium botulinum A2 str CDC 66185
Clostridium botulinum A3 str Loch Maree
Clostridium botulinumA7 str 2008–148
Clostridium botulinum A1 str ATCC 3502
Clostridium botulinum A6 str CDC 41370
FZSY033106020002
FZSY033106020003
FZSY033106030012
FZSY033106030014
FZSY033106030016
FZSY033106030018
FZSY033106030019
FZSY033106030020
Clostridium botulinum A5 str H0 4402 065
FZSY033106030013
Clostridium botulinum B4 str Eklund 17B
FZSY032906030011
FZSY032906030023
Clostridium botulinum B1 str Hall 6517(B)
Clostridium botulinum B5 str CDC 4013
Clostridium botulinum B7 str NCTC 3807
Clostridium botulinum B8 str Surat Thani 2012 (26898)
Clostridium botulinum B3 str CDC 795
FZSY033106030015
FZSY033106030021
FZSY033106030022
Clostridium botulinum B6 str Osaka05
FZSY033106030017
FZSY030506030034
Clostridium botulinum B2 str CDC 6291
FZSY030506030024
FZSY030506030026
FZSY030506030027
FZSY030506030028
FZSY030506030031
FZSY030506030032
FZSY030506030033
Bootstrap values
>90%
70%–90%
Subtpe
A4
A8
A2
A3
A7
A1
A6
A5
B4
B1
B5
B7
B8
B3
B6
B2
B
Tree scale 0.7
province
sample
Subtype
Group
ST
cftC
CBP-1
bont
closI
colA
Hemolysin
pfoA
FZSY033106030013
FZSY033106020002
FZSY033106030012
FZSY033106030016
FZSY033106030018
FZSY033106030019
FZSY033106030020
FZSY033106030014
FZSY032906030023
FZSY032906030011
FZSY033106020003
FZSY030506030026
FZSY030506030027
FZSY030506030028
FZSY030506030024
FZSY030506030033
FZSY030506030034
FZSY030506030031
FZSY030506030032
FZSY033106030017
FZSY033106030021
FZSY033106030022
FZSY033106030015
Province
Xinjiang
Qinghai
Inner Mongolia
Sample
soil
soybean
Subtype
A5(B3)
B4
B2
B3
Group
I
II
ST
98
16
NA
32
31
169
Antibiotic resistance
present
absent
Virulence-related genes
present
absent

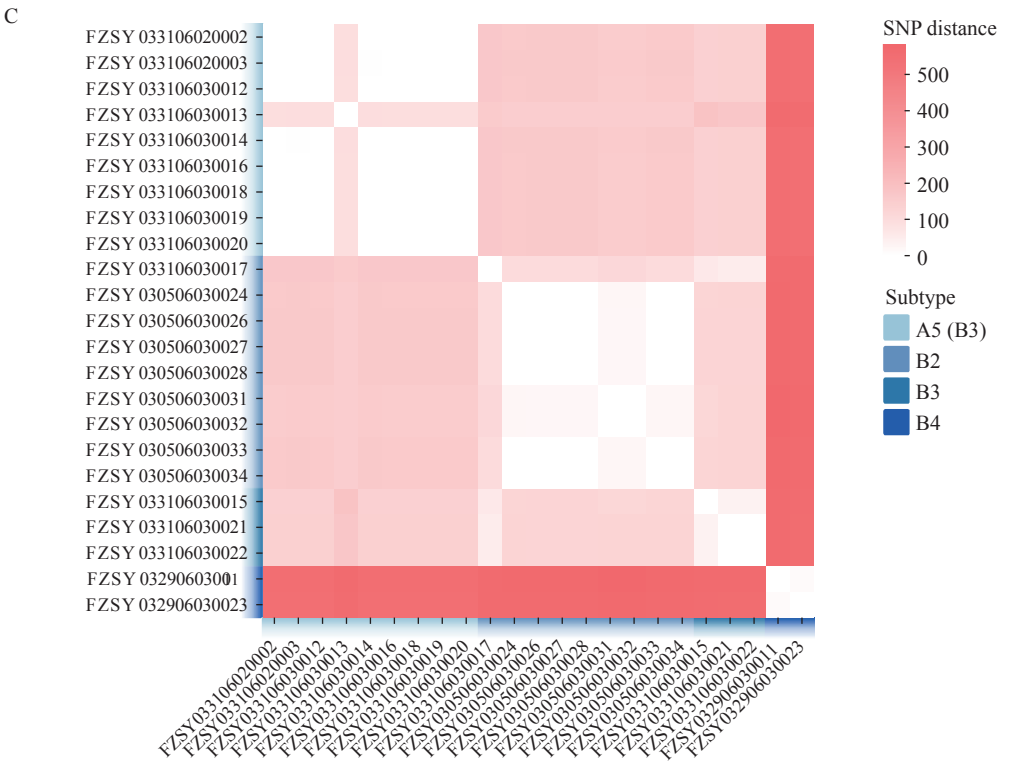

FIGURE 1. Phylogenetic analysis of 23 *Clostridium botulinum* isolates from China. (A) Neighbor-joining phylogenetic tree based on *bont* nucleotide sequences. (B) Core-genome SNP-based maximum-likelihood phylogenetic tree with a heatmap showing PLAD, sample type, subtype, multilocus sequence type, group, virulence factors, and antibiotic resistance genes. (C) SNP distance matrix illustrating pairwise genetic distances among isolates, with color gradients indicating SNP differences and subtypes.
Note: For (A) Bootstrap values (1,000 replicates) are indicated, with colors representing subtypes.
Abbreviation: SNP=single-nucleotide polymorphism; PLAD=provincial-level administrative division.

unknown functions, the most abundant categories were transcription, amino acid transport and metabolism, and cell cycle control, cell division, and chromosome partitioning (Figure 2A). Principal component analysis based on COG annotations revealed that the 23 isolates clustered into three major groups. A5(B3) and B3 exhibited functional similarities and were grouped, whereas B2 and B4 formed distinct clusters (Figure 2B). This separation was mainly driven by the categories carbohydrate transport and metabolism, transcription, and amino acid transport and metabolism (Figure 2C). Importantly, FZSY033106030013 [A5(B3)] was positioned closer to the B2 cluster, whereas FZSY033106030017 (B2) was closer to the B3 cluster.

Five virulence factors and two antibiotic-resistance genes were identified across the isolates (Figure 1B). All isolates carried *bont*, *cloSI*, *colA*, and hemolysin, whereas *pfoA* was detected only in B4 isolates. *cfrC*, encoding resistance to the antibiotics phenicol, oxazolidinone, lincosamide, and streptogramin, was present in 20 isolates but absent from both B4 isolates and one A5(B3) isolate (FZSY033106030016); CBP-1, encoding resistance to penicillin β-lactam antibiotics, was found exclusively in the B2 isolate FZSY030506030032.

Comparative analysis of the 10-kb flanking regions upstream and downstream of *bont* revealed a conserved *ha70–ha17–ha33–botR–ntnh–bont* cluster in all isolates (Figure 3). A5(B3) isolates harbored complete *bont/A5* and a truncated *bont/B3*. Two distinct gene contexts occurred within the A5(B3), B2, and B3 subtypes, with FZSY033106030013 [A5(B3)], FZSY033106030017 (B2), and FZSY033106030015 (B3) showing arrangements that differed from those of other isolates of the same subtype (Figure 3). Specifically, FZSY033106030013 [A5(B3)] contained a transposase gene and divergent downstream region, whereas FZSY033106030017 (B2) harbored a transposase gene upstream of the cluster. PHASTER analysis identified prophage sequences in all 23 genomes (Supplementary Table S4, available at

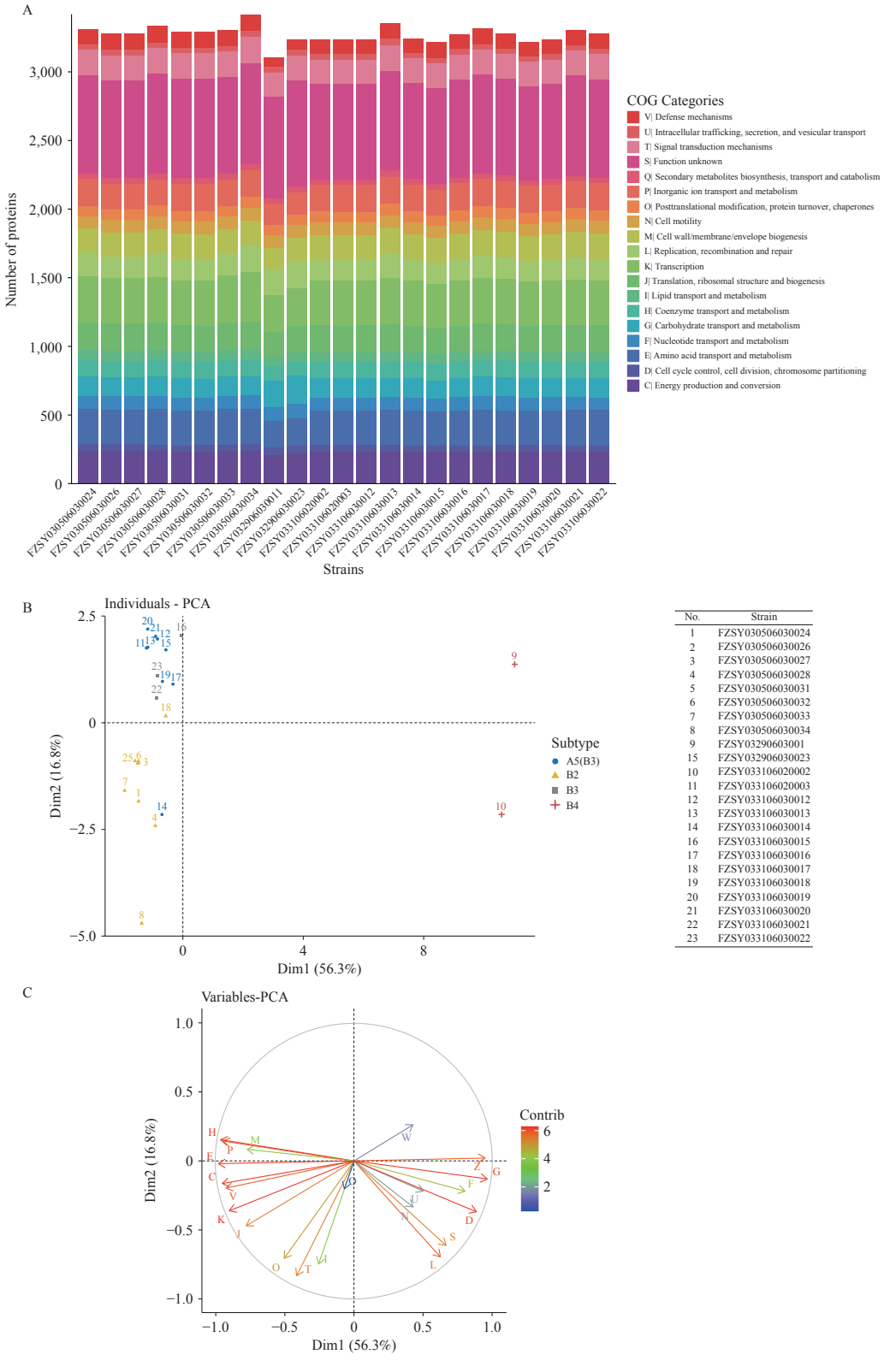

No.	Strain
1	FZSY030506030024
2	FZSY030506030026
3	FZSY030506030027
4	FZSY030506030028
5	FZSY030506030031
6	FZSY030506030032
7	FZSY030506030033
8	FZSY030506030034
9	FZSY03290603001
15	FZSY032906030023
10	FZSY033106020002
11	FZSY033106020003
12	FZSY033106030012
13	FZSY033106030013
14	FZSY033106030014
16	FZSY033106030015
17	FZSY033106030016
18	FZSY033106030017
19	FZSY033106030018
20	FZSY033106030019
21	FZSY033106030020
22	FZSY033106030021
23	FZSY033106030022

FIGURE 2. Functional annotation and PCA clustering of 23 *Clostridium botulinum* isolates based on COG categories. (A) Stacked bar chart showing the distribution of predicted proteins across 23 isolates, with colors representing COG categories. (B) PCA scatter plot of isolates along the first two principal components, with points colored by subtype. (C) PCA correlation circle plot of COG categories as variables, where arrow length and direction indicate correlation strength and sign, and color intensity indicates contribution magnitude.
Abbreviation: PCA=principal component analysis; COG=clusters of orthologous genes.

https://weekly.chinacdc.cn/), with only one isolate, FZSY033106030013 [A5(B3)], containing an incomplete prophage element that carried *bont* (Figure 4).

DISCUSSION

In China, FB cases are predominantly reported north of 30°N, with clear regional variations in the

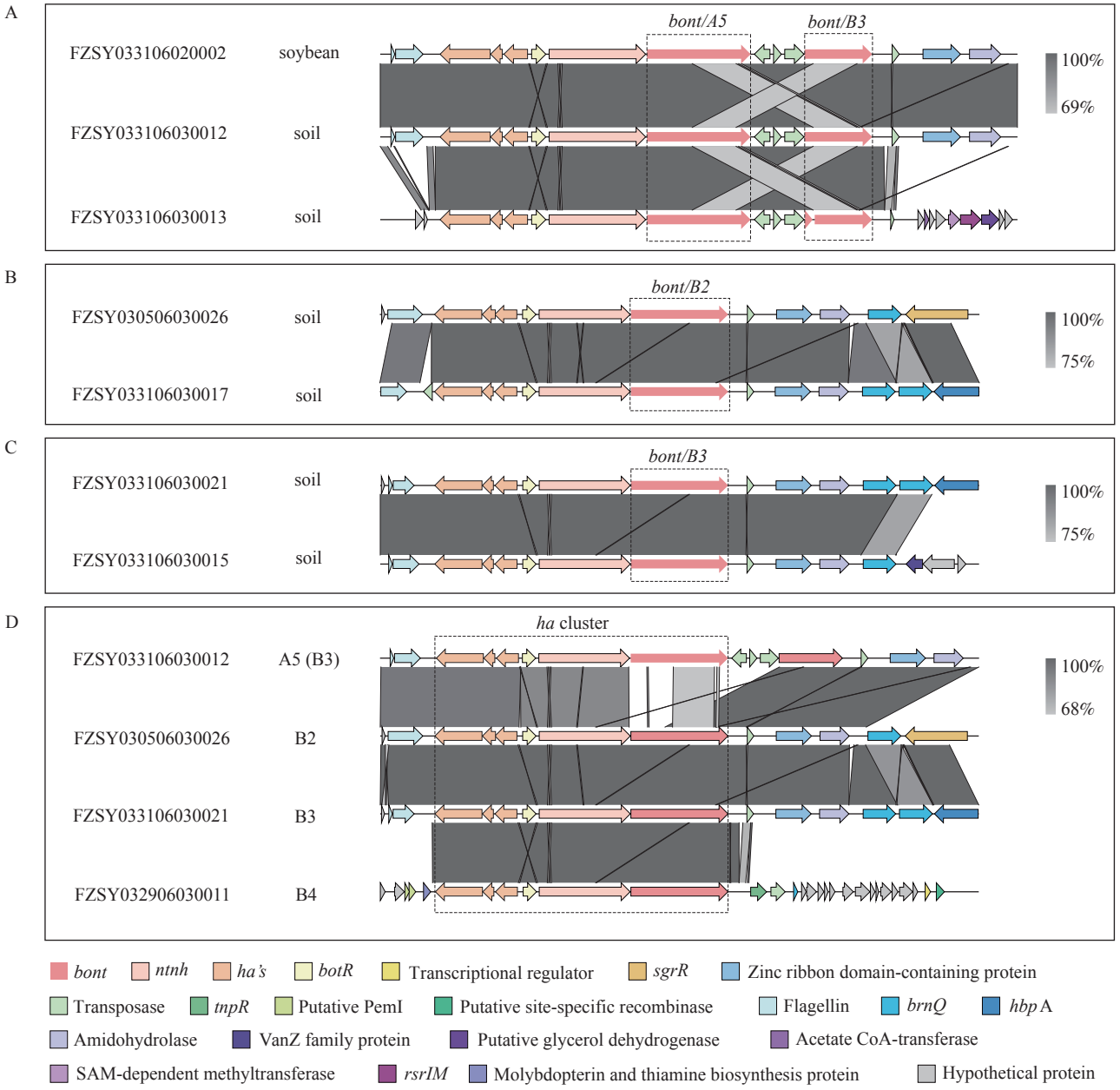

FIGURE 3. Comparative genomic context of the 10 kb upstream and downstream flanking regions of *bont* cluster in 23 *Clostridium botulinum* isolates. (A) Two distinct gene contexts of subtype A5(B3) isolates. (B) Two distinct gene contexts of subtype B2 isolates. (C) Two distinct gene contexts of subtype B3 isolates. (D) Representative gene contexts of subtypes A5(B3), B2, B3, and B4.

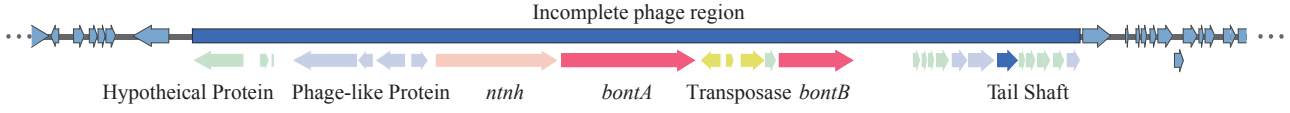

FIGURE 4. Incomplete prophage element carrying *bont* in the A5(B3) isolate FZSY033106030013.

causative foods (*9*). Homemade fermented soybean products are the primary vehicles in Xinjiang and Inner Mongolia, whereas homemade dried meats are frequently consumed in the Qinghai Plateau (*2*–*3*). Notably, recent cases of botulism were linked to commercial vacuum-packed meat and meat products, reflecting a growing concern alongside traditional sources (*5*–*6*). These products may be contaminated with soil-derived *C. botulinum* spores present on raw meat, with anaerobic packaging facilitating spore germination and toxin production. Thus, studies are needed to explore the genomic characteristics of *C. botulinum* in high-risk regions.

We collected 23 *C. botulinum* isolates from soil and soybean samples obtained from three Chinese PLADs associated with a high incidence of botulism. Phylogenetic analyses based on *bont* and cgSNPs revealed four subtypes [A5(B3), B2, B3, and B4] with distinct subtype-specific clusters. Isolates from Xinjiang and Inner Mongolia were genetically distant from those from Qinghai, suggesting geographic differentiation and adaptation to distinct ecological niches influenced by high-altitude, low-oxygen environments (*10*). Interestingly, atypical sequence types and unexpected cgSNP distances in several isolates indicate recombination or horizontal gene transfer. Importantly, the predominance of BoNT/A5(B3) in soils was consistent with the serotypes reported in historical FB cases from the same regions (*11*), suggesting that local soils act as environmental reservoirs, contributing to soil-to-food transmission. This concordance highlights the need for stricter hygiene practices in food processing, particularly during the traditional fermentation and preservation of soybean products and meat in these high-risk regions.

Functional annotation further suggested niche-specific metabolic adaptations, particularly differences in carbohydrate metabolism between subtypes, which may influence their persistence in local environments (*12*). The functional proximity of some A5(B3) and B2 isolates to other subtypes further suggested shared metabolic traits or transitional evolutionary states, possibly facilitated by genetic exchange. These ecological features, coupled with the conserved *bont* cluster and sporadic acquisition of resistance genes, support the evolutionary stability and genomic plasticity of environmental isolates (*13*). Moreover, identification of an incomplete prophage carrying *bont* suggests historical phage-mediated dissemination of toxin genes, although its current mobility remains uncertain (*14*).

This study had several limitations. First, the relatively small number of strains from the three PLADs may not fully represent the genetic diversity of *C. botulinum* across endemic regions in China. In addition, the lack of paired food and clinical isolates from outbreaks limits our ability to establish direct transmission pathways from soil to food. Finally, reliance on genomic data without phenotypic validation restricts inferences regarding toxin expression.

We performed genomic characterization of *C. botulinum* toxin subtypes from soil reservoirs in Northwest China, revealing their genomic diversity and potential ecological adaptations in high-incidence regions. Tailored surveillance and preventive strategies are needed to mitigate foodborne botulism in traditional and industrial settings.

Conflicts of interest: No conflicts of interest.

Funding: Supported by National Key Research and Development Program of China (2022YFC2303900) and Henan Medical Science and Technique Foundation (SBGJ202402091).

doi: 10.46234/ccdcw2026.038

[#] Corresponding authors: Yunchang Guo, gych@cfsa.net.cn; Xingfen Yang, yangalice79@smu.edu.cn.

[1] Food Safety and Health Research Center, School of Public Health, Southern Medical University, Guangzhou City, Guangdong Province, China; [2] China National Center for Food Safety Risk Assessment, Beijing, China; [3] Xinjiang Uygur Autonomous Region Center for Disease Control and Prevention, Urumqi City, Xinjiang Uygur Autonomous Region, China; [4] Qinghai Province Center for Disease Control and Prevention, Xining City, Qinghai Province, China; [5] Henan Province Center for Disease Control and Prevention, Zhengzhou City, Henan Province, China; [6] Inner Mongolia Center for Disease Control and Prevention, Hohhot City, Inner Mongolia Autonomous Region, China; [7] China National Institute for Food and Drug Control, Beijing, China.

Submitted: September 10, 2025
Accepted: January 12, 2026
Issued: February 27, 2026

REFERENCES

1. Rawson AM, Dempster AW, Humphreys CM, Minton NP. Pathogenicity and virulence of *Clostridium botulinum*. Virulence 2023;14(1):2205251. https://doi.org/10.1080/21505594.2023.2205251.
2. Li HQ, Guo YC, Tian T, Guo WH, Liu CQ, Liang XC, et al. Epidemiological analysis of foodborne botulism outbreaks - China, 2004-2020. China CDC Wkly 2022;4(35):788 – 92. https://doi.org/10.46234/ccdcw2022.114.

3. Wang YL, Guo XB. Epidemiological analysis of foodborne botulism in Qinghai Province from 1959 to 2022. Chin J Food Hyg 2024;36(2): 207 – 11. https://doi.org/10.13590/j.cjfh.2024.02.015.
4. Wang LJ, Li KC, Qian SY, Gao HM, Liu J, Li Z, et al. Clinical characteristics and prognosis of 8 cases of severe infant botulism. Chin J Pediatr 2024;62(3):218 – 22. https://doi.org/10.3760/cma.j.cn112140-20230908-00169.
5. Min M, Bai LL, Peng XB, Guo L, Wan K, Qiu ZW. An outbreak of botulinum types A, B, and E associated with vacuum-packaged salted fish and ham. J Emerg Med 2021;60(6):760 – 3. https://doi.org/10.1016/j.jemermed.2020.12.006.
6. Cui W, Ma CM, Liu M, Li Y, Zhou L, Shi YW, et al. Foodborne botulism caused by *Clostridium botulinum* subtype A5(b3) by self-packaged vacuum spicy rabbit heads. Microorganisms 2025;13(7):1662. https://doi.org/10.3390/microorganisms13071662.
7. Blankenberg D, Coraor N, Von Kuster G, Taylor J, Nekrutenko A, Galaxy T. Integrating diverse databases into an unified analysis framework: a Galaxy approach. Database (Oxford) 2011;2011:bar011. https://doi.org/10.1093/database/bar011.
8. Xie JM, Chen YR, Cai GJ, Cai RL, Hu Z, Wang H. Tree Visualization By One Table (tvBOT): a web application for visualizing, modifying and annotating phylogenetic trees. Nucleic Acids Res 2023;51(W1): W587 – 92. https://doi.org/10.1093/nar/gkad359.
9. Gao QY, Liu HD, Huang YF, Wu JG, Xia HQ. Foodborne botulism in China. Chin J Food Hyg 1989;(3):45-50. http://dx.doi.org/10.13590/j.cjfh.1989.03.021. (In Chinese).
10. Fu SW, Wang CH. An overview of type E botulism in China. Biomed Environ Sci 2008;21(4):353 – 6. https://doi.org/10.1016/S0895-3988(08)60054-9.
11. Shi Y, Zhao SY. Botulism in China. Mod Med J 1986;14(3):179-81. https://d.wanfangdata.com.cn/periodical/CiBQZXJpb2RpY2FsQ0hJU29scjkyMDI1MTIyNDE1NDU1NRINdGR5eDE5ODYwMzAyMhoIbzl1NjJoa2E%3D. (In Chinese).
12. Li GM, Wang HW, Zhang Y, Yan J, Duan ZW, Pang L, et al. Genomic characterisation and traceability analysis of a *Clostridium botulinum* strain involved in a food poisoning incident. BMC Infect Dis 2025;25(1):323. https://doi.org/10.1186/s12879-025-10700-4.
13. Ma X, Li KX, Li F, Su J, Meng WW, Sun YM, et al. Tracing foodborne botulism events caused by *Clostridium botulinum* in Xinjiang Province, China, using a core genome sequence typing scheme. Microbiol Spectr 2022;10(6):e0116422. https://doi.org/10.1128/spectrum.01164-22.
14. Smith TJ, Hill KK, Raphael BH. Historical and current perspectives on *Clostridium botulinum* diversity. Res Microbiol 2015;166(4):290 – 302. https://doi.org/10.1016/j.resmic.2014.09.007.

SUPPLEMENTARY MATERIAL

SUPPLEMENTARY TABLE S1. 23 *C. botulinum* isolates in this study.

Isolate ID	Origin	PLAD	Year	Subtype
FZSY033106020002	soybean	Xinjiang	2024	A5(B3)
FZSY033106020003	soybean	Xinjiang	2024	A5(B3)
FZSY033106030012	soil	Xinjiang	2024	A5(B3)
FZSY033106030014	soil	Xinjiang	2024	A5(B3)
FZSY033106030016	soil	Xinjiang	2024	A5(B3)
FZSY033106030018	soil	Xinjiang	2024	A5(B3)
FZSY033106030019	soil	Xinjiang	2024	A5(B3)
FZSY033106030020	soil	Xinjiang	2024	A5(B3)
FZSY033106030013	soil	Xinjiang	2024	A5(B3)
FZSY033106030017	soil	Xinjiang	2024	B2
FZSY030506030024	soil	Inner Mongolia	2024	B2
FZSY030506030026	soil	Inner Mongolia	2024	B2
FZSY030506030027	soil	Inner Mongolia	2024	B2
FZSY030506030028	soil	Inner Mongolia	2024	B2
FZSY030506030031	soil	Inner Mongolia	2024	B2
FZSY030506030032	soil	Inner Mongolia	2024	B2
FZSY030506030033	soil	Inner Mongolia	2024	B2
FZSY030506030034	soil	Inner Mongolia	2024	B2
FZSY033106030015	soil	Xinjiang	2024	B3
FZSY033106030021	soil	Xinjiang	2024	B3
FZSY033106030022	soil	Xinjiang	2024	B3
FZSY032906030011	soil	Qinghai	2024	B4
FZSY032906030023	soil	Qinghai	2024	B4

SUPPLEMENTARY TABLE S2. Reference *C. botulinum* genomes used for phylogenetic analysis.

Type	Name	Accession
A1	*Clostridium botulinum* str. ATCC 3502	NC_009495
A2	*Clostridium botulinum* str. CDC 66185	KM875565
A3	*Clostridium botulinum* str. Loch Maree	ABA29017
A4	*Clostridium botulinum* str. 657Ba	EU341307
A5	*Clostridium botulinum* str. H04402065	NC_017299
A6	*Clostridium botulinum* str. CDC 41370	FJ981696
A7	*Clostridium botulinum* str. 2008-148	JQ954969
A8	*Clostridium botulinum* str. 217-12	KF667385
B1	*Clostridium botulinum* str. Hall 6517(B)	EF028399
B2	*Clostridium botulinum* str. CDC 6291	EF028401
B3	*Clostridium botulinum* str. CDC 795	EF028400
B4	*Clostridium botulinum* str. Eklund 17B	X71343
B5	*Clostridium botulinum* str. CDC 4013	GU271943
B6	*Clostridium botulinum* str. Osaka05	AB302852
B7	*Clostridium botulinum* str. NCTC 3807	JN120760
B8	*Clostridium botulinum* str. Surat Thani 2012(26898)	KC714045

SUPPLEMENTARY TABLE S3. Assembly quality metrics of the 23 *C. botulinum* isolates.

Isolate ID	# contigs	Largest contig	Total length	GC (%)	N50	N90	auN	L50	L90	# N's per 100 kbp
FZSY033106020002	22	1,064,051	3,820,350	27.96	956,595	296,752	785,899.1	2	5	7.54
FZSY033106020003	26	980,537	3,816,116	27.96	948,223	140,245	639,391.4	2	7	7.49
FZSY033106030012	38	1,063,744	3,820,004	27.96	450,112	91,876	494,569.3	3	12	12.46
FZSY033106030014	30	955,337	3,841,179	27.94	542,381	91,939	533,920.8	3	9	17.6
FZSY033106030016	34	613,154	4,036,687	27.78	456,366	117,664	409,258.5	4	10	2.40
FZSY033106030018	27	1,063,876	4,033,829	27.81	957,218	140,375	688,982.3	2	7	11.80
FZSY033106030019	91	389,991	3,798,600	27.97	99,889	19,645	120,484.4	13	42	2.58
FZSY033106030020	25	1,063,877	3,818,330	27.96	956,713	140,335	723,286.4	2	6	12.54
FZSY033106030013	59	657,641	4,144,238	27.92	294,433	80,006	350,612.4	5	15	27.97
FZSY033106030017	20	1,619,332	3,954,786	27.93	763,374	359,843	960,363.8	2	5	12.21
FZSY030506030024	23	1,632,096	3,919,871	28.04	694,263	331,506	947,743.1	2	5	4.92
FZSY030506030026	31	1,622,688	3,899,509	28.08	697,890	102,244	928,959.6	2	6	14.95
FZSY030506030027	20	2,060,240	3,885,110	28.03	2,060,240	331,506	1,313,771.1	1	4	12.41
FZSY030506030028	22	1,622,773	4,093,349	27.90	734,398	208,608	910,252.0	2	6	7.11
FZSY030506030031	24	1,559,889	3,868,044	28.02	613,544	140,522	872,302.2	2	6	2.48
FZSY030506030032	26	1,560,066	3,868,479	28.02	575,595	140,522	861,060.0	2	6	5.01
FZSY030506030033	19	2,085,851	3,897,311	28.04	2,085,851	331,506	1,331,857.4	1	4	4.98
FZSY030506030034	80	2,135,297	4,230,770	28.29	2,135,297	109,580	1,227,985.7	1	7	7.00
FZSY033106030015	22	2,069,139	3,786,509	27.99	2,069,139	288,694	1,338,038.6	1	4	7.61
FZSY033106030021	32	1,121,985	4,041,323	27.83	551,067	96,717	578,130.9	3	9	16.65
FZSY033106030022	20	1,931,186	3,875,983	28.00	1,246,838	414,779	1,413,864.6	2	3	12.44
FZSY032906030011	32	675,997	3,872,241	27.16	358,211	91,935	402,042.0	4	11	4.86
FZSY032906030023	11	1,759,473	3,945,336	27.36	1,109,829	797,469	1,262,569.9	2	3	5.45

SUPPLEMENTARY TABLE S4. Summary of prophage prediction across 23 isolates.

strain	prophage regions	intact	incomplete	questionable
FZSY030506030024	5	2	2	1
FZSY030506030026	6	1	3	2
FZSY030506030027	5	1	2	2
FZSY030506030028	7	2	4	1
FZSY030506030031	3	1	2	0
FZSY030506030032	3	1	2	0
FZSY030506030033	3	1	1	1
FZSY030506030034	4	1	1	2
FZSY032906030011	7	2	3	2
FZSY032906030023	8	3	3	2
FZSY033106020002	2	1	1	0
FZSY033106020003	2	1	1	0
FZSY033106030012	2	0	1	1
FZSY033106030013	3	2	1	0
FZSY033106030014	3	1	1	1
FZSY033106030015	2	1	0	1
FZSY033106030016	4	2	0	2
FZSY033106030017	4	2	2	0
FZSY033106030018	5	0	4	1
FZSY033106030019	1	1	0	0
FZSY033106030020	2	0	1	1
FZSY033106030021	7	1	5	1
FZSY033106030022	5	2	3	0

Preplanned Studies

Comparative Transcriptome Analysis of *Bartonella* Species from Diverse Hosts Reveals Evolutionary Insights — Global, 2023–2025

Min Chen[1]; Na Han[1]; Wen Zhang[1]; Yujun Qiang[1]; Qiyong Liu[1]; Dongmei Li[1,#]

Summary

What is already known about this topic?

Transcriptomic approaches have been used in phylogenetic studies of eukaryotes, yet their application to prokaryotic organisms remains limited. To date, research on species differentiation and phylogenetic relationships within *Bartonella* spp. has relied primarily on genomic data, and the taxonomic relationships among species in this genus remain poorly resolved.

What is added by this report?

The transcriptome of *Bartonella* spp. varies based on species and host origins and exhibits systematic differences. Transcriptome-based phylogenetic analysis reveals that strains cluster by species and host origin. This pattern indicates that differentiation by species and genetic evolution of *Bartonella* is predominantly shaped by the host origin.

What are the implications for public health practice?

Our study confirms that transcriptomics is an effective tool for determining differentiation and evolutionary relationships among *Bartonella* spp. and demonstrates its potential applicability to studies of other prokaryotic species.

ABSTRACT

Introduction: To investigate transcriptional differences and their implications for evolutionary relationships among *Bartonella* species from diverse host origin.

Methods: Illumina high-throughput sequencing technology was used to sequence the transcriptomes of eighty-seven *Bartonella* strains. The differences in gene expression among strains from different species and hosts were analyzed, and the results of the genome phylogenetic analysis were compared to explore the role and influencing factors of transcription levels in *Bartonella* species differentiation.

Results: The transcriptomes of *Bartonella* strains varied systematically by species and host origin, with numerous differentially expressed genes (DEGs) identified among strains from different sources. Experimental verification confirmed that the differences in expression of *bepC*, *secB*, *secDF*, and *ftsY* played a key role in host-specific recognition. Furthermore, phylogenetic analysis based on transcriptomic data clearly reflected the taxonomic relationships among *Bartonella* species, indicating that their genetic evolution was primarily driven by host-related factors, a finding consistent with genome-based analysis.

Conclusions: Transcriptome data provides a powerful approach for clarifying species differentiation and evolutionary relationships within *Bartonella* spp., with potential applicability to other prokaryotic species. These findings provided critical insights for resolving taxonomic uncertainties and advancing systematic research.

Bartonella spp. are aerobic, fastidious intracellular parasites transmitted by arthropod vectors or through animal scratches (*1*). These pathogens exhibit broad host ranges and cause a spectrum of zoonotic diseases in humans, ranging from self-limiting infections to fatal outcomes (*1*). RNA sequencing (RNA-seq) has emerged as a powerful tool for studying the genetic evolution of species, particularly in eukaryotic phylogenetics (*2*). However, its application to phylogenetic and species differentiation studies in prokaryotes remains limited. Previous phylogenetic analyses of *Bartonella* spp. have relied on single-gene or multi-gene approaches (*3*–*4*), yet the taxonomic criteria employed in these studies remain poorly defined.

Eighty-seven *Bartonella* strains obtained from the Chinese Center for Disease Control and Prevention were analyzed (Supplementary Table S1, available at https://weekly.chinacdc.cn/). Total RNA was extracted following cultivation and used for cDNA library construction. Paired-end sequencing was performed on

the Illumina NovaSeq 6000 platform, followed by quality control, mRNA enrichment, and de novo transcriptome assembly. The assembled transcripts were functionally annotated against the Swiss-Prot, eggNOG, GO, and KEGG databases. Differentially expressed genes (DEGs) were identified using DESeq2 (|log2FoldChange|≥2, adjusted P<0.05) and subsequently subjected to GO and KEGG enrichment analyses. Single nucleotide polymorphisms (SNPs) in core genes were called from both transcriptome and genome data using Snippy (version 4.6.0, The University of Melbourne, Melbourne, Australia) and Gubbins (version 3.3.5, Wellcome Sanger Institute, Cambridge, UK), with *B. grahamii* (ATCC 700132) as the reference. Maximum likelihood (ML) and Bayesian inference (BI) phylogenetic trees were constructed using IQ-TREE (version 2.3.6, Center for Integrative Bioinformatics Vienna, Vienna, Austria) and MrBayes (version 3.2.7, Department of Biodiversity Informatics, Swedish Museum of Natural History, Stockholm, Sweden), respectively. DEGs were validated by quantitative polymerase chain reaction (qPCR) using *gltA* as the reference gene.

After quality control, 2.18 billion clean reads were obtained. De novo assembly yielded a reference transcriptome comprising 51,639 transcripts, of which 34,069 unigenes were functionally annotated. Hierarchical clustering revealed divergent gene expression patterns that correlated with host origin (Figure 1A). Strains of canine and monkey origin formed distinct clusters characterized by upregulation of class I and II genes. In contrast, rodent-origin strains exhibited heterogeneous expression profiles. Notably, numerous DEGs were identified between different species and host orders, whereas far fewer were detected within the same species or host order (Supplementary Tables S2–S3, available at https://weekly.chinacdc.cn/). Species-level DEGs were enriched in broad metabolic and information-processing categories; however, host-order-level DEGs were strikingly enriched in functions related to host interaction and pathogenesis. Specifically, significant GO terms involved host cell components, the type IV secretion system (T4SS), and immune defense mechanisms. KEGG analysis further confirmed enrichment in key pathways, including bacterial secretion and prokaryotic defense systems. Given this enrichment in host-recognition-related secretion systems, we examined the expression of these genes in detail. Key genes encoding T4SS structural components, including *virB2–4*, were significantly upregulated in strains from the order Carnivora (Table 1). qPCR confirmed significant differential expression of *bepC*, *secB*, and *secDF* (P<0.05), with trends consistent with the RNA-seq data (Figure 1B–E, Supplementary Table S4, available at https://weekly.chinacdc.cn/).

Phylogenetic analyses were conducted independently using transcriptomic and genomic datasets. For the transcriptomic and genomic analyses, 19 and 31 reference genomes were incorporated, respectively, yielding 3,498 and 24,395 core gene SNPs. Despite the difference in reference genome numbers, comparative analysis confirmed that this did not affect reconstruction reliability (Figure 2A–B). Transcriptome trees were fully resolved and exhibited strong nodal support (ML≥75%, BI≥85%). All species-level branches displayed clear species-specific clustering, revealing closely related pairs such as *B. koehlerae–B. henselae* and *B. doshiae–B. bacilliformis*. The genome-based tree also demonstrated clear species clustering with even higher support values (ML=100%, BI=100%). While interspecific relationships were largely congruent between tree types, discrepancies were observed; notably, *B. bacilliformis* clustered more closely with *B. clarridgeiae* in the genome tree. Despite these minor topological differences, species-level clade structures were highly consistent across datasets. Both ML trees exhibited clear host-associated clustering at the order level (Rodentia, Primates, and Carnivora) and at finer host-species resolution. For example, dog-associated *B. vinsonii* subsp. *berkhoffii*, cat-associated *B. koehlerae* and *B. henselae*, and monkey-associated *B. quintana* formed distinct clusters. In contrast, geographical distribution had limited influence on clustering patterns. Apart from some strains from

TABLE 1. Enrichment of differentially expressed genes in the bacterial secretion system pathway.

Groups	Status	Genes
Primates vs. Carnivora	Up	*virB6*, *virB11*, *virB2*, *virB4*, *yidC*, *virB8*, *virD4*, *sdhB*, *virB9*, *secDF*, *secY*, *tatC*, *bepC*
	Down	*lktB*, *pyrG*, *virB10*, *secA*, *ftsY*, *hrpI*, *xpsE*, *ffh*, *virB3*, *yajC*, *secB*
Primates vs. Rodentia	Up	*virB8*, *virB11*, *virD4*, *tatC*, *yajC*, *virB10*, *tatA*, *bepC*, *secDF*, *virB3*, *fliF*, *gltX1*, *secY*, *virB3*, *virB6*, *yidC*
	Down	*virB4*, *ftsY*, *pyrG*, *yidC*, *secY*, *secB*, *virB9*

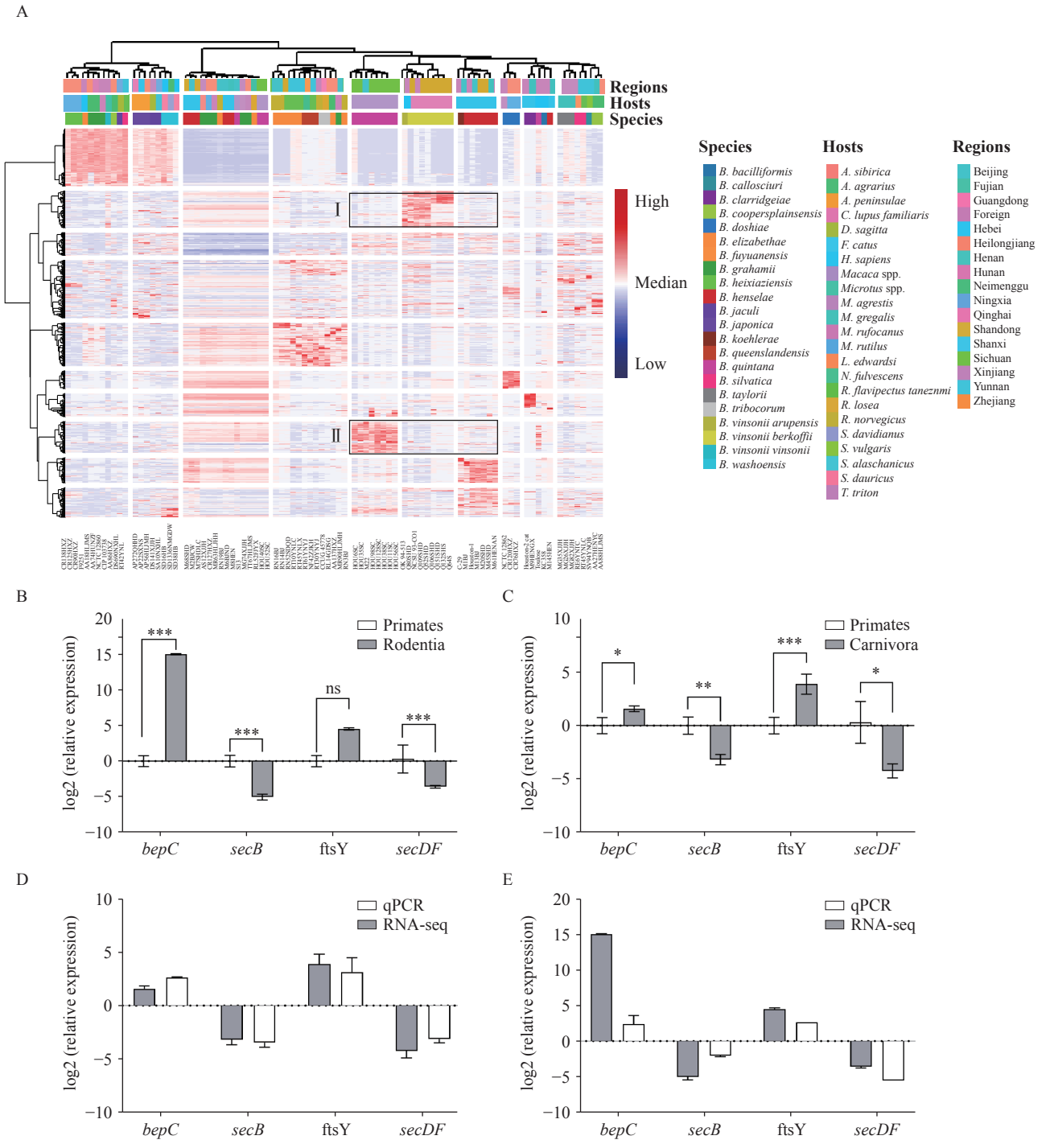

FIGURE 1. Transcriptome analysis results. (A) Gene expression clustering heatmap of 87 *Bartonella* strains. (B) qPCR validation of selected DEGs from the "Primates *vs.* Rodentia" comparison. (C) qPCR validation of selected DEGs from the "Primates *vs.* Carnivora" comparison. (D) Comparison of qPCR and RNA-seq fold-change values for the "Primates *vs.* Rodentia" comparison. (E) Comparison of qPCR and RNA-seq fold-change values for the "Primates *vs.* Carnivora" comparison.
Abbreviation: ns=not significant; qPCR=quantitative polymerase chain reaction; DEG=differentially expressed genes.
* $P<0.05$, ** $P<0.01$, *** $P<0.001$.

Sichuan and Shandong provinces forming clusters, the remaining strains showed a mosaic distribution without strong geographical signal.

DISCUSSION

Consistent with the role of gene regulation in

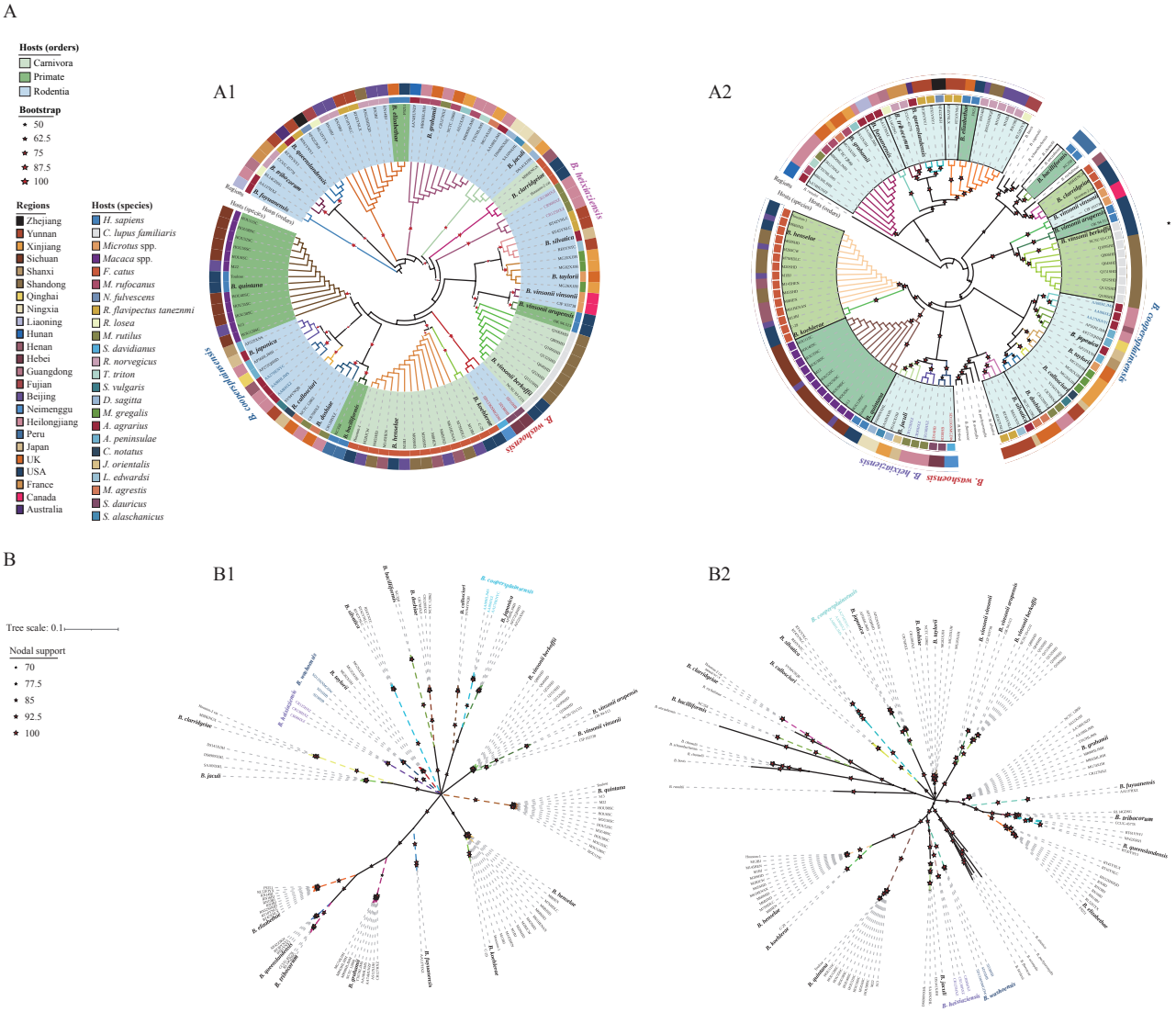

FIGURE 2. Phylogenetic trees based on core-gene SNPs. (A) ML trees constructed from transcriptomic (A1) and genomic (A2) data; (B) BI trees constructed from transcriptomic (B1) and genomic (B2) data.
Note: Branch colors indicate *Bartonella* species. Reference genomes are shown in bold; species lacking reference genomes are labeled on an outer ring with matching colors.
Abbreviation: SNP=Single nucleotide polymorphism; ML=Maximum likelihood; BI=Bayesian inference.

adaptation, hierarchical clustering revealed that *Bartonella* gene expression was conserved within species but variable between species (*5*). Furthermore, transcriptome composition differed significantly across species and host origin. Host specificity has been linked to the ability of pathogens to inject effector proteins into host cells via specialized secretion systems (*6*). Previous studies have demonstrated that *Bartonella* spp. rely primarily on the VirB/VirD4 T4SS to transport effector proteins into host cells, thereby modulating immune responses and disrupting cellular structures to promote colonization (*7*). In the present study, differential expression of *virB* and *bepC* was confirmed, and several novel host-associated DEGs were identified, including *tatC*, *tatA*, and *ftsY*. Given their implicated roles in virulence and adaptation in other pathogens, these genes may contribute to host-specific recognition in *Bartonella* spp. (*8*).

Traditional phylogenetic analyses have relied on mitochondrial and a limited number of nuclear gene markers, which are susceptible to stochastic errors (*9*). Advances in high-throughput RNA-seq now enable the application of comprehensive transcriptomic data to phylogenetic studies. In the present analysis, phylogenetic reconstruction based on core-gene SNPs from both transcriptomic and genomic data revealed

highly congruent tree topologies, validating the utility of transcriptomes for resolving taxonomic relationships within *Bartonella* spp. These analyses further revealed significant clustering of strains according to host origin, indicating that host association acted as a primary driver of species differentiation in *Bartonella* spp. In contrast to previous studies which had emphasized the role of geographic distribution in the genetic differentiation of *Bartonella*, our findings suggested that its influence was comparatively limited (*4*). This pattern could be attributed to increased cross-regional movement of host animals driven by modern socioeconomic development, which likely attenuated the impact of geographic barriers on the genetic evolution of *Bartonella* spp.

This study has several limitations. First, the limited number of strains representing certain *Bartonella* species, host types, and geographic regions may affect the generalizability of these findings. Future studies should expand the strain collection to determine whether expression profiles exhibit stronger host-specific or geographic clustering patterns. Second, the molecular mechanisms underlying the identified host-associated genes remain uncharacterized. Subsequent investigations should employ transcriptional regulation experiments to define the functional roles of these genes in host adaptation.

In conclusion, the transcriptome of *Bartonella* spp. varied systematically by species and host origin, supporting a model of host-driven speciation and evolution. This study demonstrates the utility of transcriptomics for elucidating evolutionary relationships in *Bartonella* spp. and potentially in other prokaryotes.

Conflicts of interest: No conflicts of interest.

Funding: Supported by the National Natural Science Foundation of China (31970005).

doi: 10.46234/ccdcw2026.039

[#] Corresponding author: Dongmei Li, lidongmei@icdc.cn.

[1] National Key Laboratory of Intelligent Tracking and Forecasting for Infectious Diseases, National Institute for Communicable Disease Control and Prevention, Chinese Center for Disease Control and Prevention & Chinese Academy of Preventive Medicine, Beijing, China.

Submitted: October 28, 2025
Accepted: February 23, 2026
Issued: February 27, 2026

REFERENCES

1. McCormick DW, Rassoulian-Barrett SL, Hoogestraat DR, Salipante SJ, SenGupta D, Dietrich EA, et al. *Bartonella* spp. infections identified by molecular methods, United States. Emerg Infect Dis 2023;29(3):467 – 76. https://doi.org/10.3201/eid2903.221223.
2. Jin WT, Gernandt DS, Wehenkel C, Xia XM, Wei XX, Wang XQ. Phylogenomic and ecological analyses reveal the spatiotemporal evolution of global pines. Proc Natl Acad Sci USA 2021;118(20):e2022302118. https://doi.org/10.1073/pnas.2022302118.
3. Xu AL, Lu L, Zhang W, Song XP, Li GC, Miao Y, et al. Microevolution of *Bartonella grahamii* driven by geographic and host factors. mSystems 2024;9(10):e01089 – 24. https://doi.org/10.1128/msystems.01089-24.
4. Al-Hassani MKA, Kadhim HM, Al-Galebi AAS, Gharban HAJ. First molecular phylogeny of *Bartonella bovis* in Iraqi cattle. Open Vet J 2024;14(9):2361 – 7. https://doi.org/10.5455/OVJ.2024.v14.i9.24.
5. Faure E, Kwong K, Nguyen D. *Pseudomonas aeruginosa* in chronic lung infections: how to adapt within the host?. Front Immunol 2018;9:2416. https://doi.org/10.3389/fimmu.2018.02416.
6. Wang M, Guan QX, Wang CY, Hu LY, Hu XY, Xu ML, et al. Anchorage of bacterial effector at plasma membrane *via* selective phosphatidic acid binding to modulate host cell signaling. PLoS Pathog 2024;20(11):e1012694. https://doi.org/10.1371/journal.ppat.1012694.
7. Fromm K, Ortelli M, Boegli A, Dehio C. Translocation of YopJ family effector proteins through the VirB/VirD4 T4SS of *Bartonella*. Proc Natl Acad Sci USA 2024;121(20):e2310348121. https://doi.org/10.1073/pnas.2310348121.
8. Yi X, Chen YN, Cai HY, Wang JJ, Zhang YY, Zhu ZQ, et al. The temperature-dependent expression of type II secretion system controls extracellular product secretion and virulence in mesophilic *Aeromonas salmonida* SRW-OG1. Front Cell Infect Microbiol 2022;12:945000. https://doi.org/10.3389/fcimb.2022.945000.
9. Ran JH, Shen TT, Wu H, Gong X, Wang XQ. Phylogeny and evolutionary history of Pinaceae updated by transcriptomic analysis. Mol Phylogenet Evol 2018;129:106 – 16. https://doi.org/10.1016/j.ympev.2018.08.011.

SUPPLEMENTARY MATERIAL

SUPPLEMENTARY TABLE S1. The background information of the *Bartonella* strains used in this study.

Species	Hosts	Regions	Strains
Bartonella callosciuri	*Sciurus vulgaris*	Yunnan, China	SV94YNQB
Bartonella clarridgeiae	*Felis catus*	Henan, China	M9HNGX
		USA	Houston-2 cat (ATCC 700693)
Bartonella coopersplainsensis	*Apodemus agrarius*	Henan, China	AA27HENYC
		Heilongjiang, China	AA86HXZ, AA88HLJMS
Bartonella doshiae	*Myodes rutilus*	Heilongjiang, China	CR120HXZ, CR76HXZ
	Microtus agrestis	UK	NCTC12862 (ATCC 700133)
Bartonella elizabethae	*Rattus losea*	Fujian, China	RL52FJYX
	Rattus norvegicus	Beijing, China	RN14BJ, RN16BJ, RN19BJ, RN3BJ
		Shandong, China	RN52SDQD
	Rattus tanezumi	Yunnan, China	RT10YNLC, RT45YNLX
	Homo sapiens	USA	F9251 (ATCC 49927)
Bartonella grahamii	*Apodemus agrarius*	Heilongjiang, China	AA18HLJMS
		Hunan, China	AA74HUNZF
	Allactaga sibirica	Xinjiang, China	AS12XJJH
	Myodes rutilus	Heilongjiang, China	CR127HXZ
	Microtus agrestis	Xinjiang, China	MG74XJJH
	Myodes rufocanus	Heilongjiang, China	MR63HLJHH, MR90HLJMH
	Tscherskia triton	Heilongjiang, China	TT67HLJMS
Bartonella heixiaziensis	*Myodes rufocanus*	UK	NCTC 12860 (ATCC 700132)
	Myodes rutilus	Heilongjiang, China	CR125HXZ, CR138HXZ, CR90HXZ
Bartonella henselae	*Felis catus*	Beijing, China	M13BJ, M1BJ, M2BJCW, M6BJND
		Henan, China	M145HEN, M61HENAN, M8HEN
		Shandong, China	M20SHD, M45SHDLC, M68SHDLC, M7SHDLC
		USA	Houston-1 (ATCC 49882)
Bartonella jaculi	*Dipus sagitta*	Xijiang, China	DS141XJJH
		Ningxia, China	DS690NXHL
	Spermophilus alaschanicus	Ningxia, China	SA10NXHL
Bartonella japonica	*Apodemus peninsulae*	Shanxi, China	AP22SXNS
		Qinghai, China	AP272QHHD
		Heilongjiang, China	AP56HLJMH
Bartonella queenslandensis	*Rattus tanezumi*	Yunnan, China	RT30YNYJ, RT61YNYJ
	Niviventer fulvescens	Zhejiang, China	NF42ZJKH
Bartonella quintana	*Macaca mulatta*	Sichuan, China	HOU11SC, HOU128SC, HOU35SC, HOU38SC, HOU40SC, HOU52SC, HOU56SC, HOU6SC, HOU98SC
		Beijing, China	M22, S13
Bartonella silvatica	*Homo sapiens*	USA	Toulouse (ATCC VR-358)
	Leopoldamys edwardsi	Yunnan, China	RE6YNTC
	Rattus tanezumi	Yunnan, China	RT42YNLC, RT45YNLC
Bartonella taylorii	*Microtus gregalis*	Xinjiang, China	MG26XJJH, MG35XJJH, MG82XJJH
Bartonella fuyuanensis	*Apodemus agrarius*	Heilongjiang, China	AA137HXZ

Continued

Species	Hosts	Regions	Strains
Bartonella tribocorum	*Rattus norvegicus*	France	CCUG 45778 (CIP 105476)
	Rattus losea	Guangdong, China	RL14GDSG
Bartonella vinsonii berkhoffii	*Canis lupus familiaris*	Shandong, China	Q106SHD, Q109SHD, Q132SHD, Q151SHD, Q52SHD, Q64SHD, Q80SHD
		USA	NCSU 93-CO1 (ATCC 51672)
Bartonella washoensis	*Sciurotamias davidianus*	Inner Mongolia, China	SD1336NMGDW
	Spermophilus dauricus	Hebei, China	SD16HB, SD38HB
Bartonella vinsonii arupensis	*Homo sapiens*	USA	OK 94-513 (ATCC 700727)
Bartonella vinsonii vinsonii	*Microtus* spp.	Canada	CIP 103738 (ATCC VR-152)
Bartonella bacilliformis	*Homo sapiens*	Peru	KC358 (ATCC 35685)
Bartonella koehlerae	*Felis catus*	USA	C-29 (ATCC 700693)

SUPPLEMENTARY TABLE S2. Comparative results of differentially expressed genes for strains from different *Bartonella* species.

Groups	Up	Down	Total
B. grahamii vs. B. fuyuanensis	183	176	359
B. grahamii vs. B. vinsonii berkhoffii	3,547	6,512	10,059
B. grahamii vs. B. bacilliformis	2,162	1,303	3,465
B. grahamii vs. B. callosciuri	1,316	1,656	2,972
B. grahamii vs. B. clarridgeiae	1,205	4,113	5,318
B. grahamii vs. B. coopersplainsensis	2,867	2,733	5,600
B. grahamii vs. B. doshiae	2,901	3,287	6,187
B. grahamii vs. B. elizabethae	1,991	1,783	3,774
B. grahamii vs. B. henselae	2,533	5,239	7,772
B. grahamii vs. B. quintana	2,149	4,815	6,964
B. grahamii vs. B. heixiaziensis	3,428	2,574	6,002
B. grahamii vs. B. jaculi	3,381	2,303	5,684
B. grahamii vs. B. japonica	3,316	2,479	5,795
B. grahamii vs. B. queenslandensis	968	1,676	2,644
B. grahamii vs. B. silvatica	2,378	2,474	4,852
B. grahamii vs. B. taylorii	3,888	2,324	6,212
B. grahamii vs. B. washoensis	3,889	2,425	6,314
B. grahamii vs. B. tribocorum	1,141	1,720	2,861
B. grahamii vs. B. koehlerae	2,043	2,227	4,270
B. grahamii vs. B.vinsonii arupensis	2,099	2,370	4,469
B. grahamii vs. B. vinsonii vinsonii	2,241	2,079	4,320

SUPPLEMENTARY TABLE S3. Comparative results of differentially expressed genes for *Bartonella* strains from different host origins.

Groups	Conditions	Up	Down	Total
	Orders			
Primates vs. Rodentia	/	5,863	3,068	8,931
Primates vs. Carnivora	/	4,039	3,314	7,353
Rodentia vs. Carnivora	/	3,070	10,845	13,915
	Species			
C. lupus familiaris vs. *F. catus*	Carnivora	2,699	3,291	5,990
H. sapiens vs. *M. mulatta*	Primates	432	5,364	5,796
A. agrarius vs. *M. rutilus*		2,323	3,189	5,512
A. agrarius vs. *Rattus tanezumi*	Rodentia	696	2,072	2,768
A. agrarius vs. *R. norvegicus*		1,512	3,031	4,543
	Restriction of Bartonella species			
M. agrestis vs. *M. rutilus*	*B. doshiae*	959	740	1,699
S. alaschanicus vs. *D. sagitta*	*B. jaculi*	355	177	532
N. fulvescens vs. *Rattus tanezumi*	*B. queenslandensis*	570	241	811
H. sapiens vs. *M. mulatta*	*B. quintana*	904	1,105	2,009
L. edwardsi vs. *Rattus tanezumi*	*B. silvatica*	493	1,074	1,567
S. davidianus vs. *S. dauricus*	*B. washoensis*	118	249	367
R. losea vs. *R. norvegicus*		212	11	223
R. losea vs. *Rattus tanezumi*		260	218	478
R. norvegicus vs. *Rattus tanezumi*	*B. elizabethae*	1,132	425	1557
H. sapiens vs. *R. norvegicus*		320	124	444
H. sapiens vs. *Rattus tanezumi*		1,943	210	2,153
A. agrarius vs. *A. sibirica*		1,074	493	1,567
A. agrarius vs. *M. rufocanus*		358	293	651
A. agrarius vs. *Myodes rutilus*		167	1,055	1,222
M. rufocanus vs. *Myodes rutilus*		11	441	452
M. rufocanus vs. *M. agrestis*	*B. grahamii*	13	345	358
M. rufocanus vs. *A. sibirica*		22	493	515
A. agrarius vs. *M. agrestis*		165	624	789
A. agrarius vs. *T. triton*		212	623	835
M. rufocanus vs. *T. triton*		53	364	417

SUPPLEMENTARY TABLE S4. Primer sequences for validating transcriptome reliability.

Gene name	Forward primer (5'-3')	Reverse primer (5'-3')
gltA	GGGGACCAGCTCATGGTGG	AATGCAAAAAGAACAGTAAACA
bepC	AAAGCAGCAGAGGCAGTGTATCG	TTGACGGGAAAATCTTCGGCTACG
secDF	CGCTAAGTCTTCTCGGTGCTAC	TCTTCACGGATACGCTCATTGATTAG
secB	GTGAAATTAACAACAATGGTGGAGAAC	TCCCGTGGACGCAGTGAAC
fstY	TTATGCTTGCCGCCTGTGATATG	GCATCTGCACCTAATTTTGTTGAAAC

Outbreak Reports

Field Investigation of Two Urban Cases of Severe Fever with Thrombocytopenia Syndrome — Nanjing City, Jiangsu Province, China, 2025

Xueer Wu[1,&]; Feiyan Liu[1,&]; Hengxue Wang[1]; Tao Ma[1]; Shougang Zhang[1]; Min He[1]; Zheng He[2]; Bingdong Song[1]; Xuemin Chen[1]; Songning Ding[1,3,#]; Jie Ding[1,#]

Summary

What is already known about this topic?

Severe fever with thrombocytopenia syndrome (SFTS) is a highly fatal tick-borne viral disease caused by *Dabie bandavirus* (DBV), traditionally endemic in rural agricultural and tea plantation areas. Reported cases of SFTS linked to tick bites are sparse in China's core urban areas.

What is added by this report?

This report documents two SFTS cases infected in well-afforested residential zones in the urban areas of Nanjing. Emergency tick monitoring identified DBV-positive ticks in related green spaces, suggesting the sporadic presence of natural foci in specific urban environments.

What are the implications for public health practice?

This report provides initial evidence of DBV transmission in urban areas with suitable tick habitats, which increases the risk of infection in densely populated and well-afforested urban settings. This report highlights the need for clinicians to recognize SFTS cases without a clear history of agricultural or rural exposure. To mitigate urban SFTS transmission risk, a multipronged strategy is required that encompasses strengthened surveillance, integrated vector control, public education, and clinical vigilance, including early recognition and optimized referral pathways.

ABSTRACT

Introduction: Severe fever with thrombocytopenia syndrome (SFTS) is a tick-borne viral disease caused by the *Dabie bandavirus* (DBV), which is traditionally endemic in rural agricultural and tea plantation areas. The expansion of suitable tick habitats into urban green spaces raises concerns regarding urban transmission.

Methods: In June 2025, two confirmed cases of SFTS were reported in an urban district of Nanjing, China. A Centers for Disease Control-led field investigation was conducted, including epidemiological investigations, environmental assessments, tick monitoring, and molecular analyses.

Results: Both cases involved elderly urban residents with no rural exposure or animal contact. Case 1 developed symptoms on June 11, recovered, and was discharged on June 19. Case 2 developed symptoms on June 17 and fully recovered by June 28. Neither patient experienced severe complications. At Case 2's location, tick density was 4.0 ticks/100 m·h; 83.3% (10/12) tested positive for DBV, whereas at Case 1's site, tick density was 1.25 ticks/100 m·h and all ticks tested negative. Sequencing of the L, M, and S segments showed 99.4%–100% nucleotide similarity between patient- and tick-derived strains, indicating locally acquired infection and sporadic natural DBV foci in urban environments.

Conclusion: The high DBV-positive rate in ticks from urban green spaces provides strong evidence of localized viral circulation, indicating the potential for SFTS transmission in urban environments. Our findings provide scientific support for targeted urban tick surveillance, vector control measures, and increased clinical awareness.

Severe fever with thrombocytopenia syndrome (SFTS) is a tick-borne viral disease historically confined to rural regions characterized by agricultural and tea plantation landscapes; it poses a significant threat to both human and animal health (*1*–*2*). Recent studies suggest that suitable tick habitats have expanded to urban green spaces, particularly recreational parks (*3*). In Nanjing City, Jiangsu Province, SFTS cases have shown an upward trend accompanied by geographic expansion into more

towns and subdistricts. Given the rarity of cases and limited epidemiological evidence, the risk of SFTS exposure in urban settings remains poorly understood. On June 13 and 23, 2025, two SFTS cases were reported in the urban district of Nanjing, prompting the Nanjing municipal CDC and the district CDC to initiate a field investigation. The core scientific question of this study is whether natural DBV foci exist in urban green spaces. Based on these findings, this study further evaluated the potential implications for public health strategies.

INVESTIGATION AND RESULTS

Case 1: An 82-year-old woman, reported no travel outside her residential community for 14 days before symptom onset (May 28–June 10, 2025), with only vegetable cultivation in residential garden plots. She reported no contact with patients with SFTS or their close contacts. On June 11, she developed a high fever and sought care at a tertiary hospital. The initial hematological test results were inconclusive. On June 12, her condition deteriorated and she was transferred to another tertiary hospital, where thrombocytopenia was detected (38×10^9/L). On June 13, the DBV nucleic acid test returned positive results, confirming the diagnosis of SFTS. Meanwhile, progressive thrombocytopenia was observed (14×10^9/L), accompanied by elevated cardiac enzymes, hepatic transaminases, and increased intracranial pressure. The patient was transferred to the infectious disease unit for symptomatic and supportive care. On June 19, case 1 tested negative for DBV nucleic acids test and was discharged. The complete epidemiological timeline is illustrated in Figure 1A.

Case 2: A 75-year-old man, lived approximately 1.2 km north of the patient in Case 1. Two weeks before illness onset (June 3–16, 2025), he had no travel or mountain excursions but reclaimed unmanaged grassland within his residential area for vegetable cultivation. He reported no contact or close contact with patients with SFTS. On June 17, he developed a fever and visited a community health center on June 18. Initial tests revealed mild thrombocytopenia (107×10^9/L). Despite symptomatic treatment, his condition persisted with fever and worsening thrombocytopenia (86×10^9/L), prompting referral to a tertiary hospital on June 20. Nucleic acid testing confirmed DBV infection on June 21. From June 20–22, his platelet count further declined (75×10^9/L), accompanied by diarrhea, abdominal pain, and generalized myalgia. Case 2 received daily infusion

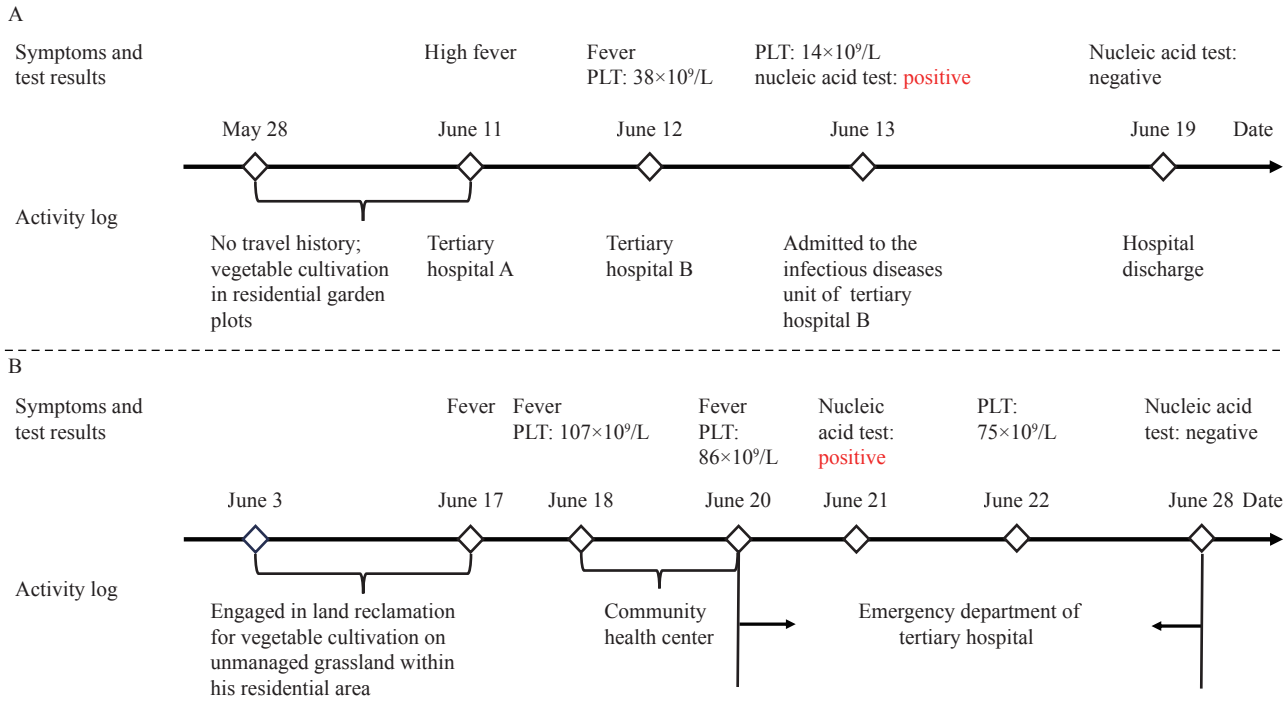

FIGURE 1. Epidemiological timeline of two SFTS cases in urban area — Nanjing City, Jiangsu Province, China, 2025. (A) Case 1; (B) Case 2.
Abbreviation: PLT=platelet; SFTS=severe fever with thrombocytopenia syndrome.

therapy in the hospital emergency department until June 28 when the nucleic acid test was negative (Figure 1B).

Both patients reside in foothill neighborhoods in central urban areas. (Figure 2A). Case 1's residential complex included 13 buildings, 180 households, and approximately 350 residents. Case 2's residential complex comprised 27 buildings, 1,000 households, and over 3,000 residents. Both communities featured abundant grassland and shrub vegetation suitable for tick habitats.

The municipal and district CDCs conducted tick surveillance on June 14 and 23 in areas associated with two confirmed SFTS cases. Sampling sites were selected based on the national vector surveillance guidelines issued by the China CDC, which prioritize grassy patches and low shrubs within the daily activity zones. Tick collection was performed at 9∶30 a.m. to avoid direct sunlight exposure. Three trained field investigators participated in each of the sampling sessions. Eight sites were sampled, including vegetable plots, grassy slopes at the foot of the mountains, residential green spaces, forest edges, and walking paths (Figure 2B). A standardized flagging method using a 90 cm × 60 cm white flannel cloth combined with manual capture was employed. At each sampling site, dragging was conducted along predefined transects for a distance of at least 500 meters and for a duration of at least 30 minutes. The collected ticks were stored in tubes until further testing. Tick density was calculated as ticks per 100 meters per person-hour (ticks/100 m·h). A total of 17 ticks were collected. All the five ticks from Case 1's sampling sites (density: 1.25 ticks/100 m·h) were tested negative for DBV. However, 10 of the 12 ticks obtained from Case 2's sampling sites (4 ticks/100 m·h) were DBV-positive using Reverse Transcription-Polymerase Chain Reaction (RT-PCR). Morphological identification was performed according to the "Handbook for Classification and Identification of Main Vectors", using features such as body segments, mouthparts, and legs (*4*). By comparing these characteristics with reference atlases, the predominant ticks were confirmed to be *Haemaphysalis longicornis*. Ticks were found in green spaces surrounding the patients' residences, which coincided with their routine walking paths. DBV-positive ticks were detected within approximately 100 meters of the residence in Case 2 and within approximately 500 meters of the residence in Case 1. Neither case reported recent contact with animals or pet ownership. Although some residents of the community owned dogs, no tick infestation was observed upon examination of the animals' ears.

Viral RNA was extracted from patient serum samples and tick homogenates, and DBV was detected using real-time RT-PCR. Whole-genome sequencing

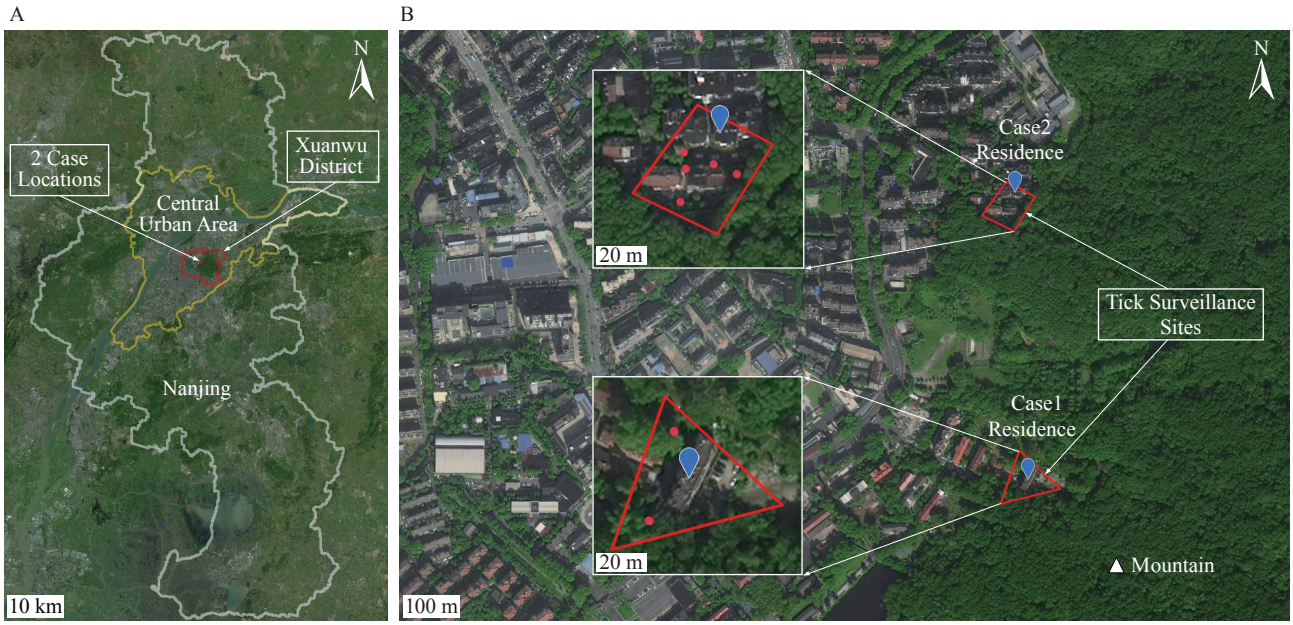

FIGURE 2. Geographic locations and environmental features of the two SFTS cases in Xuanwu District, central Nanjing City, Jiangsu Province. (A) Geographic location of Xuanwu district in Nanjing city; (B) Geographic distribution of two cases and surveillance sites.
Abbreviation: SFTS=severe fever with thrombocytopenia syndrome.

was performed using a bunyavirus whole-genome capture kit (Hangzhou Baiyi Technology Co. Ltd., China). Sequencing libraries were prepared using a Nextera XT kit (Illumina, USA) and sequenced on an Illumina MiniSeq platform using a High Output Reagent Kit (300 cycles). Raw reads were assembled using CLC Genomics Workbench 22.0.2. Only assemblies with an average depth ≥100× and genome coverage ≥90% were retained. Sequence alignment and homology analysis were performed using MEGA 5.2. Sequence analysis demonstrated that the viral strains from Case 1 shared 99.7%, 99.7%, and 99.4% nucleotide similarity with the tick-derived strains in the L, M, and S segments, respectively. In Case 2, sequencing of the L segment was unsuccessful; however, the M and S segments showed 99.9% and 100% similarity, respectively, with the strains isolated from tick monitoring. The results showed a high degree of genetic consistency between patient- and tick-derived DBV strains.

PUBLIC HEALTH RESPONSE

A series of strategies and measures have been implemented in Nanjing to control the prevalence of SFTS in urban areas (Figure 3). Generally, multiple local departments swiftly mounted coordinated responses. The responses focused on personnel management, tick control, and environmental remediation. These were supported by targeted health education and collaboration across sectors and were adapted to urban settings.

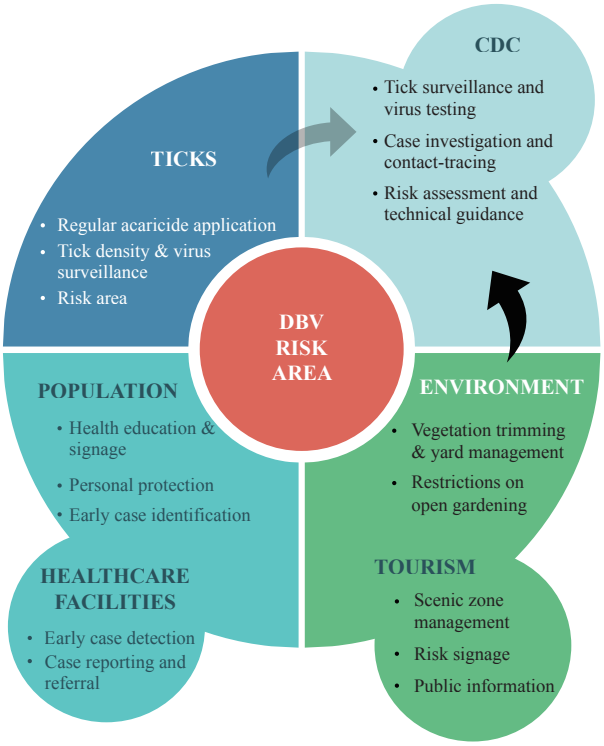

FIGURE 3. Multi-level infection control strategy for urban SFTS cases.
Abbreviation: DBV=*Dabie bandavirus*; SFTS=severe fever with thrombocytopenia syndrome.

In terms of personnel management, occupational protection training was provided to the scenic area staff and migrant workers, and household outreach was conducted among local residents. The public was advised to adopt personal protective behaviors and deworm pets regularly to reduce exposure to ticks. Tick control measures have targeted common urban tick habitats, including mountain trails, residential gardens, and green belts. Routine acaricide application was implemented along with ongoing surveillance of tick density and DBV positivity to support precise risk area delineation. Additionally, preventive tick control measures were implemented in other urban areas with similar ecological characteristics. Environmental remediation involves clearing potential tick-breeding sites and installing warning signs to reduce the exposure risk. Health education was conducted through community engagement, scenic area broadcasts, and new media platforms to raise awareness among residents and tourists.

DISCUSSION

Through combined epidemiological and microbiological evidence, this report documents cases of locally acquired SFTS in the urban core of a major city in China. Both patients were elderly residents living in central Nanjing whose daily activities were confined to walking within residential green spaces and cultivating vegetables in community gardens. They had no recent travel to rural or hilly endemic areas and had no history of SFTS or animal contact. Environmental surveillance detected DBV-positive ticks approximately 100 meters from the residence in one case, and sequence analysis demonstrated a high degree of genetic consistency between the patient- and tick-derived strains. These findings strongly suggest that natural foci of DBV may have established sporadically in urban environments, highlighting an emerging infection risk for foothill neighborhood residents and the particular vulnerability of elderly individuals with reduced mobility in well-vegetated urban communities.

Since its discovery, SFTS has mainly been reported

in rural areas dominated by agricultural and tea plantation areas (*5*–*6*). Ecological changes have recently facilitated the expansion of tick habitats into urban areas, raising concerns about urban transmission (*3*). In 2024, 6 locally acquired SFTS cases were reported in Beijing's rural–urban fringe. Although DBV-positive ticks and hedgehogs were detected in urban parks in Beijing, no such cases were reported in urban core areas, possibly because of the low abundance of *Haemaphysalis longicornis* (*7*). In contrast, the present study provides the first systematic evidence supporting local transmission and the probable establishment of natural foci within a densely populated and highly urbanized city center. This distinction may reflect variations in urban ecological structure and different stages of tick vector adaptation across metropolitan environments. However, the occurrence of urban cases does not necessarily indicate a recent introduction of the virus into the city but may also reflect previously unrecognized or under-detected transmission under suitable ecological conditions. Therefore, continuous surveillance and systematic risk assessment are essential for accurately characterizing the extent and intensity of urban transmission. Despite the urban setting, several characteristics of the present cases were consistent with those reported in rural SFTS studies. Both infections occurred during the typical seasonal peak. *Haemaphysalis longicornis* was identified as the predominant tick species, and exposure was linked to low-vegetation outdoor environments. These consistencies indicate that the fundamental transmission pattern of SFTS remains unchanged, despite the urban context.

Nanjing experiences a subtropical monsoon climate with hot and rainy summers (*8*–*9*). Ongoing urban greening initiatives have resulted in a persistently high vegetation coverage. Urban green spaces, including scenic areas, recreational parks, and community landscapes, are widely distributed across cities and frequently overlap with residential environments. Nanjing is situated along the East Asian-Australasian flyway through which migratory birds regularly pass and interact with local urban ecosystems (*10*). Together, these climatic and ecological characteristics may act as key driving forces that facilitate tick survival, host availability, and viral maintenance in urban environments. The combination of favorable microclimatic conditions, abundant urban green spaces, and the introduction of infected ticks via migratory birds may jointly promote the establishment and persistence of urban DBV natural foci (*11*–*13*). Nevertheless, the relative contributions and interactions of these drivers warrant further investigation through multi-season and multisite ecological and pathogen surveillance studies.

Although urban transmission remains rare, this study has important implications for public health. First, it highlights the need to establish standardized diagnostic and treatment pathways for SFTS in urban areas. Clear protocols for case recognition, testing, treatment, referral, and reporting should be developed to ensure a timely diagnosis and appropriate case management. Training healthcare providers is necessary to strengthen early detection and rapid responses. Second, tick surveillance should be implemented in urban scenic areas and parks to assess the tick density and DBV prevalence, with priority given to zones with previously documented infections. Scenic spots, parks, and residential communities in urban areas should also be prioritized for environmental remediation. Third, targeted health education should be conducted in scenic spots and well-greened residential communities, including setting up warning signs and posters and strengthening awareness of SFTS protection and healthcare-seeking behaviors among urban residents.

This study was subject several limitations. First, the small number of confirmed urban cases and tick samples limit the generalizability of our findings. Second, although ticks were investigated, systematic surveillance of potential animal hosts in urban environments was not conducted, restricting our ability to fully characterize the local transmission cycle of DBV. Third, the limited sample size precluded a comprehensive phylogenetic analysis, preventing the reconstruction of the evolutionary history of the virus and its relationship with other known strains. Future studies with expanded tick and animal host sampling, combined with long-term surveillance, are needed to better understand DBV maintenance, transmission pathways, and the evolving risk of SFTS in urban areas. Additionally, with a larger sample size, phylogenetic analyses can be performed to further elucidate the evolutionary history of the virus and its relationship with other regional and global strains.

Conflicts of interest: No conflicts of interest.

Funding: Supported by the Research and Innovation Project of the Nanjing Institute of Public Health, Nanjing Medical University (NCX2304).

doi: 10.46234/ccdcw2026.040

[#] Corresponding authors: Songning Ding, njcdcdsn@stu.njmu.edu.cn; Jie Ding, E-yu2an2002@163.com.

[1] Nanjing Municipal Center for Disease Control and Prevention, Nanjing City, Jiangsu Province, China; [2] Xuanwu District Center for Disease Control and Prevention, Nanjing City, Jiangsu Province, China; [3] School of Public Health, Nanjing Medical University, Nanjing City, Jiangsu Province, China.
[&] Joint first authors.

Submitted: December 31, 2025
Accepted: February 24, 2026
Issued: February 27, 2026

REFERENCES

1. Cui HL, Shen SJ, Chen L, Fan ZY, Wen Q, Xing YW, et al. Global epidemiology of severe fever with thrombocytopenia syndrome virus in human and animals: a systematic review and meta-analysis. Lancet Reg Health West Pac 2024;48:101133. https://doi.org/10.1016/j.lanwpc.2024.101133.
2. Liu WS, Dai K, Wang T, Zhang HY, Wu JH, Liu W, Fang LQ. Severe fever with thrombocytopenia syndrome incidence could be associated with ecotone between forest and cultivated land in rural settings of central China. Ticks Tick Borne Dis 2023;14(2):102085. https://doi.org/10.1016/j.ttbdis.2022.102085.
3. Yi B, Fan MQ, Chen J, Yao JY, Chen X, Liu HX. An alarming public health problem: ticks and tick-borne pathogens in urban recreational parks. China CDC Wkly 2025;7(16):553 – 60. https://doi.org/10.46234/ccdcw2025.091.
4. Zhou MH, Chu HL. Handbook for classification and identification of main vectors. Suzhou: Soochow University Press. 2019. https://book.kongfz.com/1219849/9390509741. (In Chinese).
5. Miao D, Liu MJ, Wang YX, Ren X, Lu QB, Zhao GP, et al. Epidemiology and ecology of severe fever with thrombocytopenia syndrome in China, 2010–2018. Clin Infect Dis 2021;73(11):e3851 – 8. https://doi.org/10.1093/cid/ciaa1561.
6. Huang XX, Li JD, Li AQ, Wang SW, Li DX. Epidemiological characteristics of severe fever with thrombocytopenia syndrome from 2010 to 2019 in Mainland China. Int J Environ Res Public Health 2021;18(6):3092. https://doi.org/10.3390/ijerph18063092.
7. Yuan F, Zhu LL, Tian D, Xia MY, Zheng MH, Zhang Q, et al. The first discovery of severe fever with thrombocytopenia virus in the center of metropolitan Beijing, China. Virol Sin 2024;39(6):875 – 81. https://doi.org/10.1016/j.virs.2024.11.002.
8. China Meteorological Administration. Nanjing geographic and climatic characteristics. 2014. https://www.cma.gov.cn/2011xzt/2014zt/20140730/2014073002/201407300201/201408/t20140802_254423.html. [2026-1-16]. (In Chinese).
9. Nanjing Municipal Committee, Nanjing Municipal People's Government. Natural conditions of Nanjing. 2025. https://www.nanjing.gov.cn/zjnj/zrzk/. [2026-1-16]. (In Chinese).
10. Shen W, Zhao ZX, Xu ZP, Zhang Y. Occurrence dataset of birds in the Xinjizhou National Wetland Park, Nanjing, China. Biodivers Data J 2023;11:e103497. https://doi.org/10.3897/BDJ.11.e103497.
11. Yuan JM, Su J, Zhang ZH, Sun B, Jiao XL, Zhang X, et al. Initial study and phylogenetic analysis of hard ticks (Acari: Ixodidae) in Nantong, China along the route of avian migration. Exp Appl Acarol 2024;92(4):871 – 83. https://doi.org/10.1007/s10493-024-00916-5.
12. Zhang DW, Sun CK, Yu HY, Li JX, Liu WD, Li ZF, et al. Environmental risk factors and geographic distribution of severe fever with thrombocytopenia syndrome in Jiangsu Province, China. Vector Borne Zoonotic Dis 2019;19(10):758 – 66. https://doi.org/10.1089/vbz.2018.2425.
13. Zhang X, Zhao CY, Si XX, Hu Q, Zheng AH. Natural circulation of tick-borne severe fever with thrombocytopenia syndrome virus in the city ecosystem, China. Virol Sin 2023;38(5):832 – 5. https://doi.org/10.1016/j.virs.2023.08.004.

Notes from the Field

Fatal Human Rabies in an HIV-Infected Migrant Worker with Well-Controlled Viral Load — Zhejiang Province, China, January 2026

Zhiping Long[1,&]; Miaofen Lou[2,&]; Xuelian Zhang[1]; Yi Wang[2]; Kaizhi Bai[1]; Zhifeng Pang[1]; Guangming Zhang[1,#]

In January 2026, a 53-year-old male migrant worker was diagnosed with fatal rabies in Zhejiang Province, China. The patient had a documented 10-year history of human immunodeficiency virus (HIV) infection and was receiving regular antiretroviral therapy with Biktarvy. At the time of hospital admission, laboratory testing on January 12 demonstrated effective virological control, with a CD4+ T-lymphocyte count of 335 cells/μL and an undetectable HIV-1 viral load; however, syphilis serology was positive. The patient had recently returned to Jinhua City, Zhejiang Province, from Tongren City, Guizhou Province, in December 2025.

Approximately 4 months prior to symptom onset, on September 10, 2025, the patient sustained a bleeding finger bite from his domestic dog while residing in Songtao County, Guizhou — a known rabies-endemic area (*1*). Critically, no post-exposure prophylaxis (PEP) was administered following this exposure (*2*). The dog was slaughtered and consumed shortly after the incident. On January 8, 2026, the patient developed influenza-like symptoms that rapidly progressed. By January 10, symptoms had evolved to include vertigo and limb weakness. Given his immunocompromised status, initial differential diagnoses focused on neurosyphilis and HIV-associated opportunistic infections. Targeted next-generation sequencing (tNGS) of cerebrospinal fluid (CSF), performed by Hangzhou Adicon Clinical Laboratories, failed to identify a pathogen.

On January 16, the emergence of pathognomonic rabies symptoms — hypersalivation and hydrophobia — prompted urgent reassessment. Unbiased metagenomic next-generation sequencing (mNGS) of the CSF, also conducted by Hangzhou Adicon Clinical Laboratories, successfully identified rabies virus (RABV) RNA, establishing a definitive diagnosis of furious rabies. The patient died on January 17 (Figure 1). This case illustrates how concurrent HIV infection and syphilis can obscure the early clinical recognition of rabies, while demonstrating the critical diagnostic value of mNGS in resolving complex, atypical presentations of infectious encephalitis.

Upon laboratory confirmation, the Jinhua CDC initiated an epidemiological investigation that identified 23 close contacts. Contact classification included family caregivers (n=6), healthcare workers (n=10), and community members (n=7; comprising five individuals who consumed the dog meat, one funeral handler, and one sanitation worker). All contacts underwent standardized risk assessment and received PEP in accordance with national rabies prevention guidelines.

Because the exposure event occurred retrospectively in Guizhou Province, the precise number of villagers participating in the dog slaughtering could not be definitively established. All identified high-risk individuals were nevertheless counseled to initiate PEP. A cross-provincial notification was transmitted to the Guizhou CDC to enable coordinated source investigation and contact tracing efforts. As of February 2026, no secondary transmission has been documented. All close contacts remain under active surveillance for a minimum of 6 months, consistent with national rabies prevention protocols.

This case demonstrates critical challenges in diagnosing rabies when concurrent conditions complicate clinical presentation. First, clinicians evaluating patients with acute neurological symptoms should systematically elicit detailed animal exposure histories, particularly in individuals with immunocompromising conditions such as HIV infection. Co-morbidities can mask pathognomonic rabies features, delaying recognition even in patients with well-controlled viral loads (*3*–*4*). Second, when conventional diagnostic approaches fail to identify causative pathogens in unexplained encephalitis, unbiased mNGS provides a powerful tool for detecting rabies virus and other atypical neurotropic pathogens (*5*). Third, rabies-endemic rural areas require

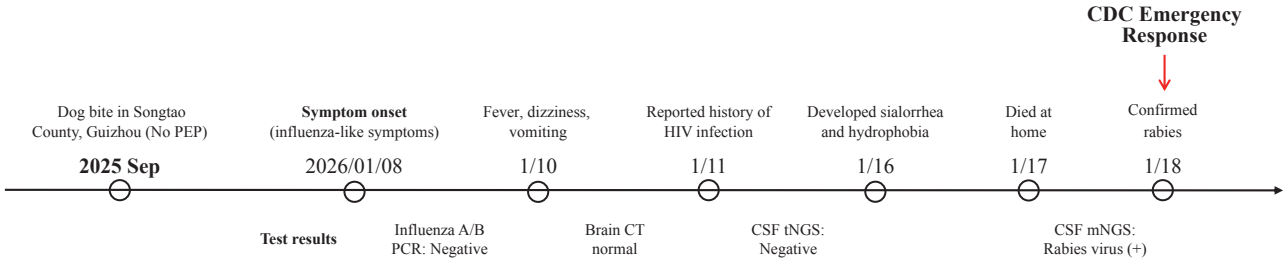

FIGURE 1. Timeline of exposure, symptom onset, diagnostic evaluation, and clinical outcome in a fatal human rabies case with HIV co-infection, Zhejiang Province, China.
Abbreviation: CSF=cerebrospinal fluid; CT=computed tomography; HIV=human immunodeficiency virus; mNGS=metagenomic next-generation sequencing; PCR=polymerase chain reaction; tNGS=targeted next-generation sequencing; PEP=post-exposure prophylaxis.

strengthened public health infrastructure to ensure timely PEP access and effective risk communication campaigns that explicitly discourage slaughtering and consuming animals suspected of rabies infection. Finally, protecting migrant worker populations demands coordinated interprovincial surveillance systems, standardized contact tracing protocols, and targeted health education initiatives implemented in both labor-exporting and labor-receiving regions to address the unique vulnerabilities of mobile populations.

Conflicts of interest: No conflicts of interest.

doi: 10.46234/ccdcw2026.041

[#] Corresponding author: Guangming Zhang, zgmacn@outlook.com.

[1] Jinhua Center for Disease Control and Prevention, Jinhua City, Zhejiang Province, China; [2] Wucheng District Center for Disease Control and Prevention, Jinhua City, Zhejiang Province, China.
[&] Joint first authors.

Submitted: February 05, 2026
Accepted: February 23, 2026
Issued: February 27, 2026

REFERENCES

1. Li HY, Li YJ, Chen Y, Chen B, Su Q, Hu Y, et al. Mapping rabies distribution in China: a geospatial analysis of national surveillance data. Int J Infect Dis 2023;131:140 – 6. https://doi.org/10.1016/j.ijid.2023.04.002.
2. Hampson K, Coudeville L, Lembo T, Sambo M, Kieffer A, Attlan M, et al. Estimating the global burden of endemic canine rabies. PLoS Negl Trop Dis 2015;9(4):e0003709. https://doi.org/10.1371/journal.pntd.0003709.
3. Fooks AR, Banyard AC, Horton DL, Johnson N, McElhinney LM, Jackson AC. Current status of rabies and prospects for elimination. Lancet 2014;384(9951):1389 – 99. https://doi.org/10.1016/S0140-6736(13)62707-5.
4. Clifford DB, Ances BM. HIV-associated neurocognitive disorder. Lancet Infect Dis 2013;13(11):976 – 86. https://doi.org/10.1016/S1473-3099(13)70269-X.
5. Wilson MR, Sample HA, Zorn KC, Arevalo S, Yu GX, Neuhaus J, et al. Clinical metagenomic sequencing for diagnosis of meningitis and encephalitis. N Engl J Med 2019;380(24):2327 – 40. https://doi.org/10.1056/NEJMoa1803396.

Youth Editorial Board

Indexed by Science Citation Index Expanded (SCIE), Social Sciences Citation Index (SSCI), PubMed Central (PMC), Scopus, Chinese Scientific and Technical Papers and Citations, and Chinese Science Citation Database (CSCD)

The inauguration of *China CDC Weekly* is in part supported by Project for Enhancing International Impact of China STM Journals Category D (PIIJ2-D-04-(2018)) of China Association for Science and Technology (CAST).

CHINA CDC WEEKLY

CCDC weekly

Vol. 8 No. 9 Feb. 27, 2026

中国疾病预防控制中心周报(英文)

Responsible Authority
National Disease Control and Prevention Administration

Sponsor
Chinese Center for Disease Control and Prevention

Editor-in-Chief
Jianwei Wang

Editing and Publishing
China CDC Weekly Editorial Office
No.155 Changbai Road, Changping District, Beijing, China
Tel: 86-10-63150501, 63150701
Email: weekly@chinacdc.cn

Printing: Beijing Kexin Printing Co., Ltd

Complimentary Access

CSSN
ISSN 2096-7071 (Print)
ISSN 2097-3101 (Online)
CN 10-1629/R1